TECHNISCHE UNIVERSITÄT WIEN

Vienna University of Technology

MASTER THESIS

Prediction of biomass slagging behaviour in fluidized bed reactors based on ternary diagrams

Carried out for the purpose of obtaining the degree of Master of Science (MSc), submitted at TU Wien, Faculty of Mechanical and Industrial Engineering, by

Christophe JEZIERSKI

Matr.Nr.:1623335

under the supervision of

Univ. Prof. Dipl.-Ing. Dr. techn. Hermann Hofbauer

and co-supervision of

Dipl.-Ing. Sebastian Diem

Insitute of Chemical, Environmental and Bioscience Engineering

Vienna, November 4, 2018

Affidavit

I declare in lieu of oath, that I wrote this thesis and performed the associated research myself, using only literature cited in this volume.

Vienna, November 4, 2018   Signature

Acknowledgement

First of all, I would like to thank Prof. Hofbauer for building up this master thesis to my taste from scratch. It was really nice to work with fluidized bed reactor, a technology I never had the chance to work with. I am taking as well this opportunity to thank him for welcoming me at TU Wien and the support that he gave me during the whole master even with his busy schedule.

Secondly, I really want to show my infinite appreciation to Sebastian Diem. Thank you so much for the support along this thesis from the start till the end especially with the experiments. Although, some experiments didn't go as planned, he stayed positive and he overcame troubles along the way. Without him, this master thesis couldn't have been accomplished.

Abstract

In the context of greenhouse gases reduction, biomass represents a promising alternative to fossil fuels. However, biomass has some inconvenients in combustion systems. One of those practical problems in fluidized bed reactors is bed agglomeration caused by fused ash sticking bed particles together. This phenomena is commonly called "slagging".

In this master thesis, the potential of ternary diagrams as prediction method for biomass slagging tendency was investigated. Ternary diagrams are generally powerful thermodynamic tools because they enable to make decisions without doing any experiment. However, a preliminary literature research showed that ternary diagrams are mostly used for classification purpose and not as an established prediction method. The limits of ternary diagrams are first the availability of data and secondly, the prediction accuracy. Indeed, in these ternary systems, the ash composition is approximated to the sum of the main oxides. By neglecting the other components, the melting temperature predicted is generally way higher than the one measured by Ash Fusion Test (AFT) for example because these components contribute to decrease the melting temperature. Thus, further developments are needed to extract the most out of this potential prediction method.

In the practical part of this thesis, the combustion of olive pellet was performed in a lab-scale fluidized bed reactor provided by the Institute of Chemical, Environmental and Bioscience Engineering at TU Wien. The experiment was performed two times in order to check results consistency. The bed agglomeration was detected at 950 ℃ approximatively when bed temperature and pressure under the bed decrease. The pressure drop can be explained by agglomerates formation which offer a bigger counter-pressure to the air pressure. The bed temperature decreases because the combustion efficiency goes down due to agglomerates formation. The bed temperature (950 ℃) measured at the agglomeration time is between the deformation temperature (840 ℃) and the flow temperature measured by AFT (1400 ℃) which is what was expected.

Contents

Chapter 1

Introduction

1.1 European context

The EU has committed to reduce its greenhouse gas emissions (GHG's) to 80-95% below the 1990 levels, by 2050. This commitment requires changes on social, economical, institutional and technological aspects. All those requirements are summarized in the Energy roadmap 2050 which mentioned the scenarios towards a secure, competitive and decarbonised energy system by 2050. One of the important point mentioned by the roadmap, is the increasing contribution of renewable energies to global energy consumption reaching 75% by 2050. According to predictions, the current efforts contribute to reduce emissions only by about 40% by 2050 [European commission, 2012]. As we can see in figure 1.1, the total share of renewable energy to the overall energy consumption was 18,2% in 2016 compared to 79,5% for fossil fuels meaning that additional efforts are absolutely needed.
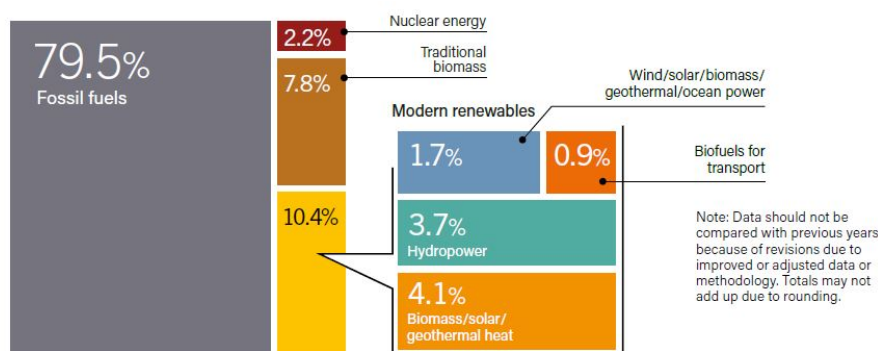

Figure 1.1: Renewable share of total final energy consumption in 2016 [REN21, 2018]

1.2 Biomass as a renewable energy source

According to "Renewables 2018-Global status report", solid biomass represented 12,8% of the total share of biomass in renewable energy in 2016 (see figure 1.2).

A differentiation has to be made between the traditional and modern use of biomass. On one hand, the traditional use involves the combustion of biomass to provide heat via low-efficient stoves to households in developing countries. On the other hand, modern use provides heat at larger scale to be used directly or to be converted into power via combined heat and power (CHP) cycle for residential, commercial and industrial customers. Therefore, combustion of biomass (both traditional and modern) is one important process for heat production and proves the relevance of the topic.
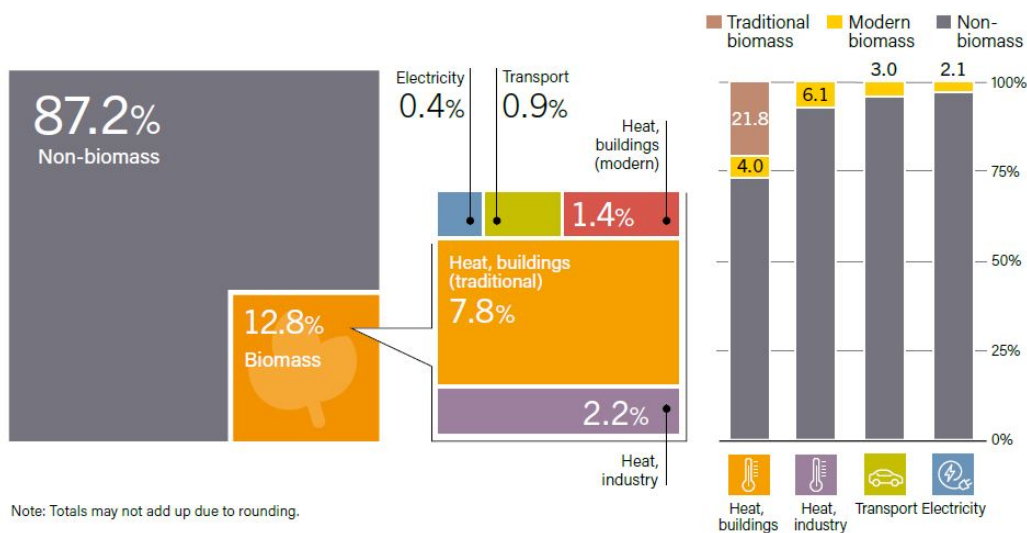

Figure 1.2: Shares of biomass in total final energy consumption, overall and by-end use sector in 2016 [REN21, 2018]

1.3   Biomass definition

The EU directive [EU, 2001] defined the biomass as "the biodegradable fraction of products, waste and residues from agriculture (including vegetal and animal substances), forestry and related industries, as well as the biodegradable fraction of industrial and municipal waste".

[Vassilev et al., 2012] gives a more precise composition-based definition: "Biomass is contemporaneous (non-fossil) and a complex biogenic organic-inorganic solid product formed by natural and anthropogenic (technogenic) processes, and comprises: natural constituents originated from growing land- and water-based vegetation via photosynthesis or generated via animal and human food digestion; and technogenic products derived via processing of the above natural constituents. Biomass similar to solid fossil fuels, is a complex heterogeneous mixture of organic matter and, to a less extent, inorganic matter, containing various solid and fluid intimately associated phases. The phases in biomass originate from natural (authigenic and detrital) and anthropogenic processes"

As table 1.1 shows, the term comprises plenty of products from different origins, compositions and phases. Several classification methods have been proposed in the literature, one of them is based on biological diversity, source and origin which makes the difference between types of biomass classified by the authors as wood and woody biomass, herbaceous and agricultural biomass, aquatic biomass, animal and human wastes, contaminated biomass and industrial biomass wastes called "semi-biomass" and biomass mixtures.

Table 1.1: General classification of biomass varieties as solid fuel resources according to their biological diversities, sources and origins [Vassilev et al., 2012]

Biomass groups	Biomass sub-groups, species and varieties
1. Wood and woody biomass	Coniferous or deciduous, angiospermous or gymnospermous and soft or hard such as stems, barks, branches (twigs), leaves (foliage), and others from various wood species
2. Herbaceous and agricultural	Annual or perennial, arable or non-arable and field-based or processed-based biomass from various species such: grasses and flowers (alfalfa, arundo, reed canary, others), straws (barley, bean, others), stalks (alfalfa, arthar, arundo, others), fibers (coconut coir, flax, others), shells and nuts (almond, cashewnut, coconut, others), pits (apricot, chery, olive, others) and other residues from various species (fruits, pips, others)
3. Aquatic biomass	Marine or freshwater, macroalgae or microalgae and multicellular or unicellular species (blue, blue-green, brow, golden, green and read algae: diatoms, duckweed, giant brown kelp, seaweed, sweet-water weeds, water hyacinth, others)
4. Animal and human biomass wastes	Bones, chicken litter, meat-bone meal, sponges, various manures, others
5. Industrial biomass wastes	Municipal solid waste, demolition wood, refuse-derived fuel, sewage sludge, hospital waste, paper-pulp sludge, water papers, paperboard waste, chipboard, fibreboard, plywood, wood pallets and boxes, railway sleepers, tannery waste, other
6. Biomass mixtures	Blends from the above varieties

1.4 Problem situation

Considering the current european regulations and the major contribution of bioenergy to the overall renewable energy sources (RES) share, biomass will play a major role to reduce GHG's. However, although biomass is providing lots of future opportunities, some technological challenges inherent to biomass composition hamper the development of current combustions technologies. Thus, most of the mineral compounds remain as residues in form of ashes in combustion systems during combustion of solid biofuels. Those mineral residues have a low sintering or melting temperature leading to slag or clinker formation causing damages and therefore, increasing maintenance costs.

This problem for now has not found yet a proper solution for fluidized bed reactor applications. One solution proposed in the literature is to add additives to shift the melting temperature towards higher temperatures levels. Unfortunately, the understanding of relevant processes is quite scarce and research is still underway.

Some methods exist to characterize and to predict the melting behaviour based on an approximation of ash composition like ternary diagrams. The latter has been used in some literature papers mostly as classification tool but is not yet classified as "well-established" prediction method. This master thesis will have the task to prove the potential of ternary diagram as method to predict slagging tendency of biomass ash. First, a thorough literature research will be performed to have a better understanding of the problematic in the chapter 2. The chapter 3 proposed a summary of the current ternary diagrams used in the literature. In the chapter 4, fluidized bed reactor experiments at the Institute of Chemical, Environmental and Bioscience Engineering under the direction of Univ. Prof. Dipl.-Ing. Dr. techn. Hermann Hofbauer have been performed to compare results with literatur research. The chapter 5 proposes a short summary of the main results and learning points of the work.

Chapter 2

Current state of art: Ash melting behaviour

The use of biomass, as an alternative to fossil fuels, generates other technical issues due to its differences in terms of composition compared to fossil fuels like coal. Thus, the following practical problems in biomass combustors can occur during combustion (see figure 2.1):
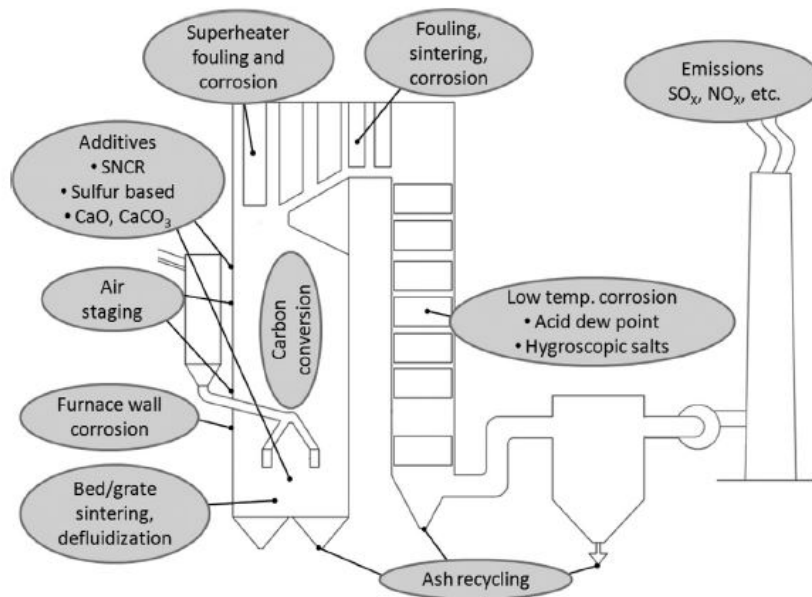

Figure 2.1: Technical issues encountered in combustion processes related to biomass composition [Hupa et al., 2017]

One of the problems mentioned by [Hupa et al., 2017] is bed/grate sintering defluidiza-tion caused by "slagging". This phenomenon is defined as the formation of molten ash which can generate bed particles agglomeration in a fluidized bed reactor unabling the combustor to perform at its optimal conditions and deteriorating its integrity. The source of slagging resides in the presence of inorganic components like potassium and sodium in biomass forming low-melting materials. Melting behaviour of biomass ashes has been documented extensively in the literature. However, the understanding of the main phenomena is still ongoing and efficient counter-measures to prevent or to mitigate related problems are yet to be found.

The goal of chapter 2 is to summarize the current understanding of ash melting be-haviour in scientific literature on different aspects: composition, current technologies to characterize ash melting behaviour and standards, correlations used to predict slagging and fouling tendencies, problems happening in conversion technologies and current so-lutions found. Another aim of this chapter is to provide readers with an enough amount of knowledge to understand chapter 3 which addresses ternary diagrams.

2.1   Ash composition and behaviour

Ash is a mineral residue formed by thermochemical reactions happening during the com-bustion. The major ash-forming elements are Si, Ca, Na as well as K, P, Mg, nutrients for plants, which are distributed between the biomass itself and ash already contained in the fuel. Ca and Mg increase ashes melting temperature and K and Na decrease it. Indeed, when Si reacts with K and Na it forms silicates having a low melting point causing slagging and deposition on combustors surfaces.

One of these big challenges of predicting ash melting temperature resides in the high variety of biomass types (see table 1.1). Indeed, the combustion of two biomass types will produce ashes having of course the same ash forming elements but not in the same proportion which complexifies the studies of ash behaviours in a combustor. As figure 2.2 shows, the distribution of ash forming elements can be radically different from one type of biomass to another.
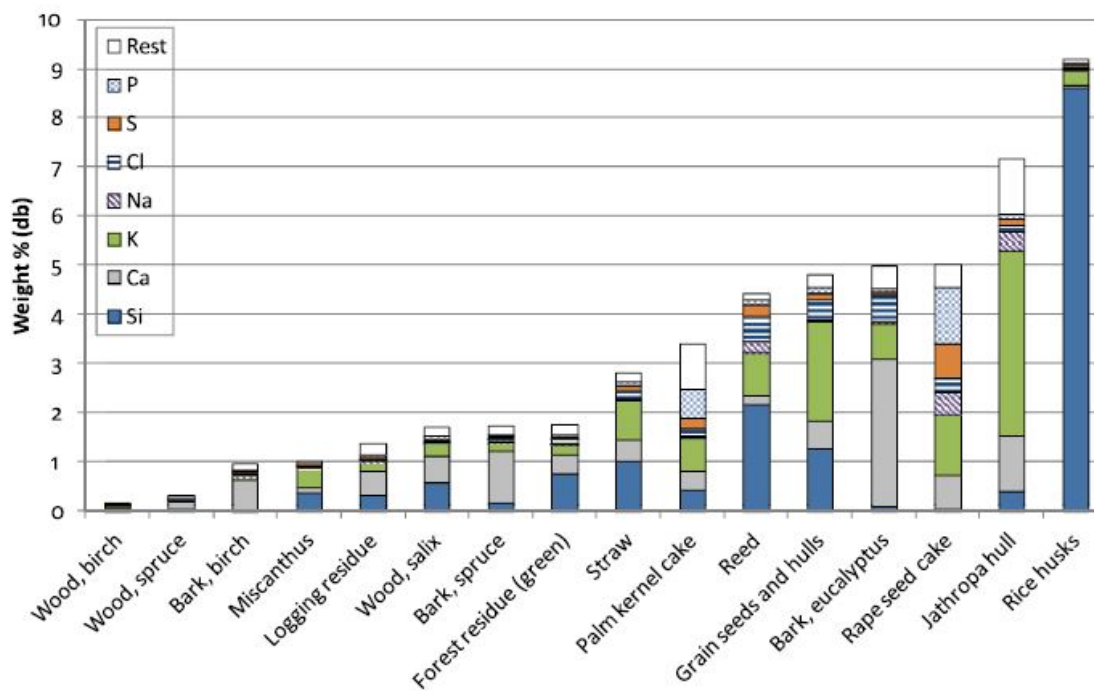
Figure 2.2: Ash forming elements in different types of biomass [Hupa et al., 2017]

2.2 Current analytical and prediction methods for ash melting behaviour

Several analytical and prediction techniques currently exist to characterize the melting behaviour of ash at high temperatures: ash fusion test (AFT), simultaneous thermal analysis (STA), empirical correlations, ternary diagrams and thermodynamic modeling.

2.2.1 Ash fusion test

The Ash fusion test (AFT) is based on the determination of four characteristic temperatures defined according to standards.

Concretly, a test piece made of ash from a certain shape is initially prepared and then heat up in a furnace according to a constant temperature gradient. The physical principles as well as the overall look of heating microscope are given in figures 2.3 and 2.4.

The piece shape evolution is continuously observed by a microscope (see figure 2.5).
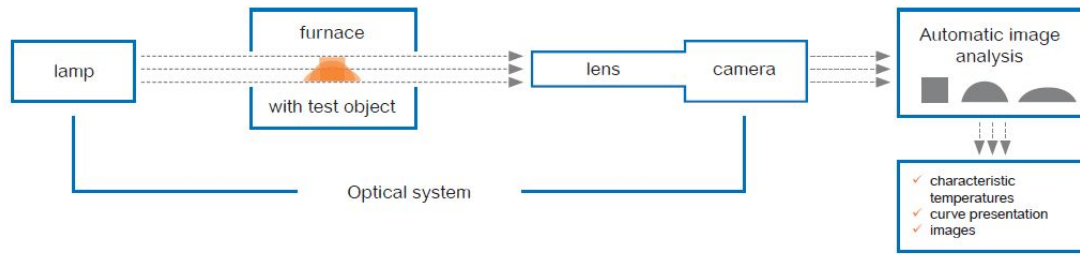
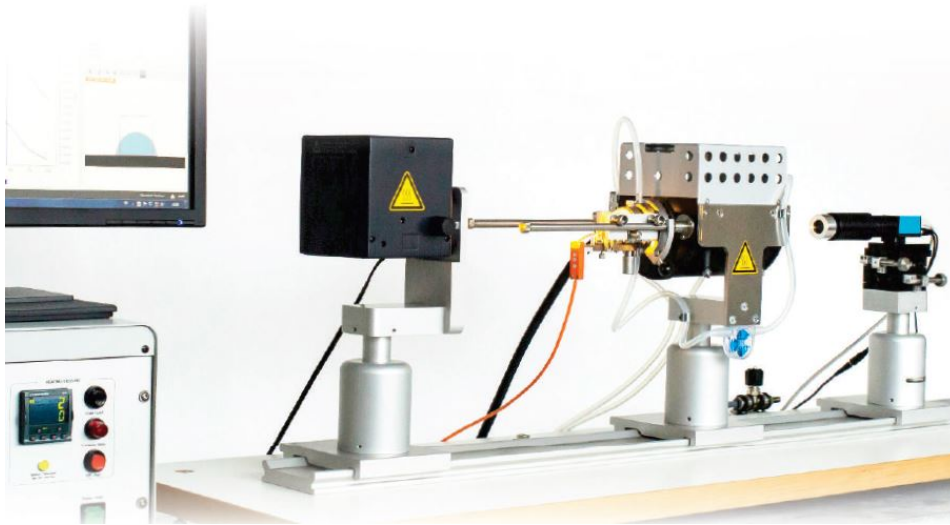Figure 2.3: Ash fusion test instrument physical principle [Hesse intruments, 2016]

Figure 2.4: Ash fusion test instrument [Hesse intruments, 2016]
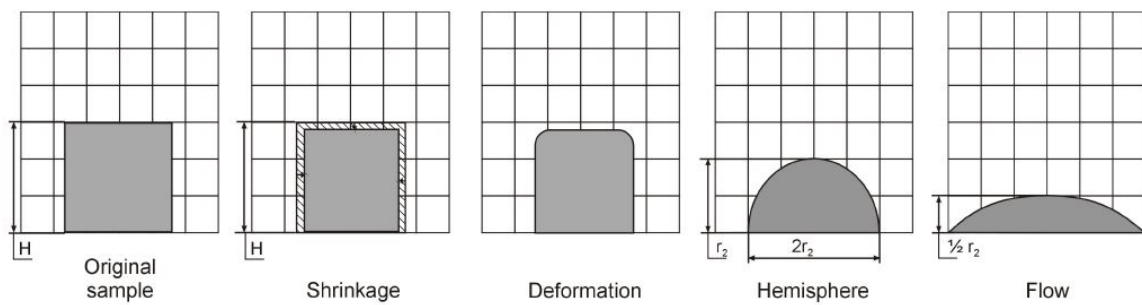

Figure 2.5: Ash piece shape evolution (original shape and size at 550 °C) [CEN/TS 15370-1, 2006]

The following characteristic temperatures defined by the standard CEN/TS 15370-1 are:

- Shrinkage temperature (SST): temperature at which shrinking of the test piece occurs. This temperature is defined as when the area of the test piece falls below 95% of the original test piece area at 550 ℃,

- Deformation temperature (DT): temperature at which the first signs of rounding of the edges of the test piece occurs due to melting,

- Hemisphere temperature (HT): temperature at which the test piece forms approximately a hemisphere i.e. when the height becomes equal to half the base diameter,

- Flow temperature (FT): temperature at which the ash is spread out over the supporting tile in a layer, the height of which is half of the height of the test piece at the hemisphere temperature.

Some authors mentioned to be careful regarding values of temperatures obtained by this laboratory test because of its high variability. The high discrepancies in terms of results is due to different ways of performing ash melting analysis and the lack of clarity concerning the temperatures definitions. Current work like [Wojcik et al., 2018] have been realized to identify limits of CEN/TS 15370-1 standards and align laboratories around the same experimental protocol.

Other standards exist as well like the german standard DIN 51730 [DIN 51730, 2007] for fossil fuels which differs from CEN/TS 15370-1 [CEN/TS 15370-1, 2006] in terms of specimen shapes, ways of preparing ashes, ash binder, size of particles, heating procedure and the definition of the characteristic temperatures. Therefore, ash fusion temperature technique solely doesn't provide enough clues to take a decision regarding slagging propensity of a certain type of ash. This test should be therefore coupled with other analytical methods in order to get a complete overview.

2.2.2   Simultaneous thermal analysis

Simultaneous thermal analysis (STA) refers to the use of thermogravimetry (TGA) and differential scanning calorimetry (DSC) in the same instrument.

Thermal gravimetric analyis (TGA) is an analytic method measuring the mass change of a sample submitted to temperature changes under a controlled atmosphere over time. It provides useful information about physical phenomena over the temperature range considered. Concretly, the sample located is a furnace where the temperature can be adjusted according to a certain program. The mass change of the sample is measured by a high precision balance. As the temperature varies, the percentage of initial mass is reported as function of the time or temperature, each inflexion point corresponding to a physical transformation or reaction.

Next to TGA, differental scanning calorimetry (DSC) is a thermoanalyisis method measuring the heat required to increase the temperature as the same rate as a reference which has a well-defined heat capacity. DSC supports TGA for phase transition identification. Indeed, as the temperature of the sample increases linearly, it undergoes physical tranformation either realeasing or requiring heat (exothermic or endothermic reaction). Therefore, more or less heat needs to be provided or removed in order to maintain the temperature increase at the same rate as the reference. By measuring the heat flow difference between sample and reference, DSC is able to measure the heat absorbed or released during the reaction. The energy input required to maintain the temperature constant is reported for each time or temperature, each peak is related to one physical transformation or reaction in particular.

These two analytical methods are usually in parallel to identify univoquely phase transitions/chemical reactions happening in a sample over a temperature range by comparing both diagrams obtained. As far as ash melting behaviour is concerned, a TGA/DSC diagram is given as example at the figure 2.6.
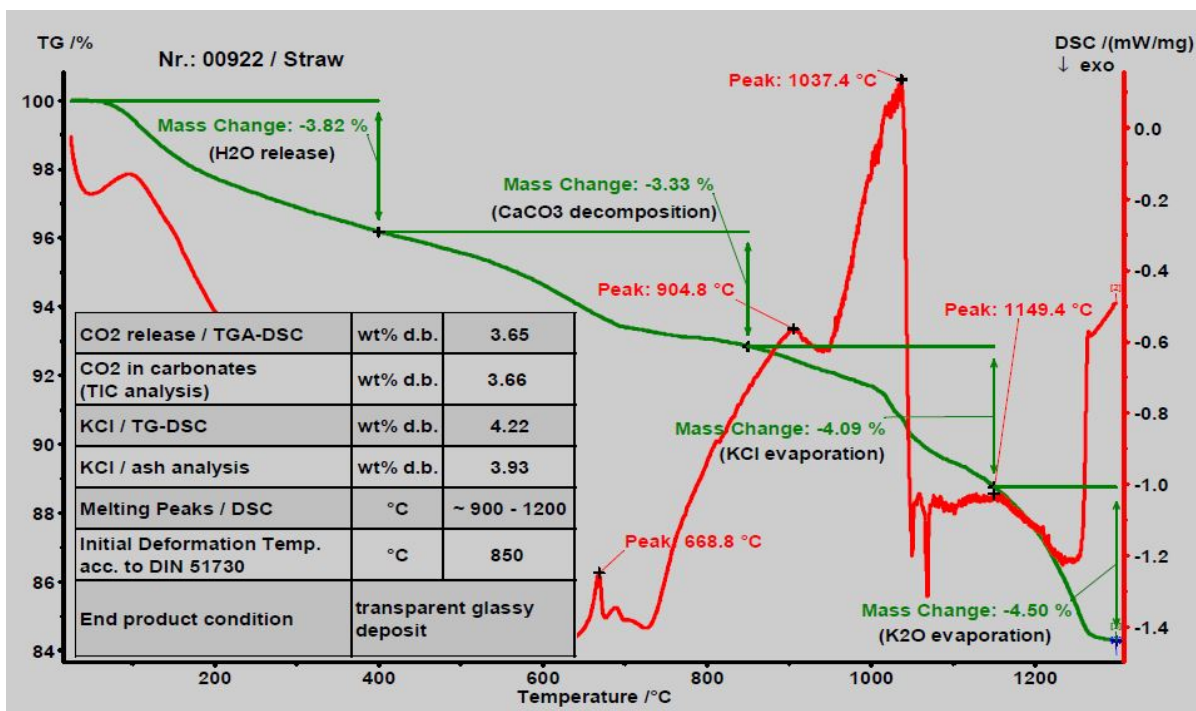
Figure 2.6: Results of STA for straw ash [Glarborg et al., 2013]

Straw ash has a composition mainly consisting of silicon and potassium with small amount of chlorine and sulfur causing problems in combustion systems. The straw sample was ashed at 550 ℃ and the latter was submitted to STA for analysis.

The following TGA and DSC diagrams have been determined. An emphasis on relevant parts of diagrams has been underlined:

- Till 400 ℃: evaporation of crystal water,

- 400-850 ℃: endothermic peak corresponding to $CaCO_3$ decomposition and release of CO_2,

- 850-1150 ℃: KCl evaporation,

- Endothermic peaks at 905, 1037 ℃ can be assigned to different ash melting phases,

- 1150 ℃ endothermic peak which might be explained by K_2O release.

STA measured the beginning of ash melting at around 900 ℃ which is 50 ℃ higher than the melting temperature determined by AFT, 850 ℃. The reason of such difference can be found in the section 2.2.1 regarding standards for AFT.

2.2.3 Existing correlations

The use of fuel indices can help us as well to characterize biomass fuels. Those indices are calculated based on fuel data analyses and allow the experimenter to study interactions between different elements contributing to the slagging tendency. Concretly, they describe the relation between temperature of slag and proportions between acid and basic components. The important ash forming elements are K, Na, Ca, Mg, S and Cl.

Regarding ash melting properties, it is known that Ca and Mg increase melting temperature and Si combined with K reduces it on the contrary. For ash systems containing Si, Ca, Mg and K, the melting tendency is given by the Si/(Ca+Mg) molar ratio. For systems containing P, the molar ratio is slightly different (Si+P+K)/(Ca/Mg). The idea is to compare the proportion of elements reducing or increasing ash melting point and based on the ratio value, make a conclusion. When both fuel indexes are inferior 1, melting temperature can be considered as high. On the other hand, low ash melting tempratures inferior to 1000 °C such as straw have Si/(Ca+Mg) and (Si+P+K)/(Ca/Mg) ratios superior to 2,5 and 5 respectively.

These indexes have the advantage to be easily used for pre-evaluation of fuels because they are calculated directly from fuels data. However, although they are easy to use, attention is required regarding the interpretation of the results. Indeed, the results are based from the real-scale combustion meaning that results are dependent from the combustion technologies. Therefore, the reference data need to be checked in order to compare results. Secondly, indexes have been evaluated for a particular range of biomass compositions. Again, attention is required concerning potential extrapolations.

In conclusion, ash melting indexes have an acceptable accuracy for pre-characterization of fuels and get an idea of some trends. However, results from this methods, in order to be comparable, should be from comparable combustion technologies and compositions as the considered correlation supposed.

2.2.4   Ternary diagrams

Ternary diagrams are usually a powerful tool in science. In our case, ash melting temperature can be predicted based on ternary diagrams as well. Each composition in the diagram corresponds to a triplet of compositions. Solidus and liquidus curves are usually shown as well enabling to predict temperatures at which ashes begin to melt.

By reporting the point on the diagram of the system considered, one can see how the composition evolves when the temperature changes and what kind of problematic compounds can be formed at operating temperature. More details on ternary diagrams are to be found in the chapter 3.

2.2.5   Thermodynamic modeling

Thermodynamic models and databases are used to predict the chemistry of ash-forming elements in biomass during combustion. For equilibrium calculations, several software tools exist on the market (see table 2.1). However, accuracy and consistency of phases and species thermodynamic data are still problematic and limit their usage.

Thermodynamic modeling is used to predict equilibrium of multi-components systems like biomass ash in our case. The calculations are based on the minimization of Gibbs energy which are possible only if thermodynamic data exist for all phases considered like chemical potential for each component present in the system.

$$G = \sum_i n_i G_i$$

Where G is the Gibbs energy of the mixture, G_i is the Gibbs energy of the component i and n_i is the amount of the component i .

For mutlicomponent and multiphase equilibria calculations in thermochemical processes, FactSage is one of the most commonly used software amongst other (see table 2.1). FactSage is able to deal with complex phase diagrams calculations and contains an extensive database for thermochemical processes like molten salt and slag chemistry.

Table 2.1: Thermodynamic modeling softwares for ash chemistry [Lindberg et al., 2013]

Thermodynamic software	Own database	Complex solutions	Special features
ChemApp	No	Yes	User-defined programming library for custom-made application
ChemSheet	No	Yes	Spreadsheet application for customized process modeling
FactSage	Yes	Yes	Contains extensive databases for molten salts and slags
HSC	Yes	No	Contains extensive thermodynamic databases for stoichiometric compounds
MTDATA	Yes	Yes	Contains extensive databases for molten salts and slags
Thermo-Calc and DICTRA	Yes	Yes	Contains extensive databases for metallurgical applications and can be used for simulating diffusion-controlled phase transformations

2.3 Slagging problems in biomass conversion technologies

The ash forming elements, mentioned above, can undergo a variety of physical transformations and chemical reactions depending on chemical composition as well as combustion temperature and residence time. Two categories of transformations can be identified (see figure 2.7).
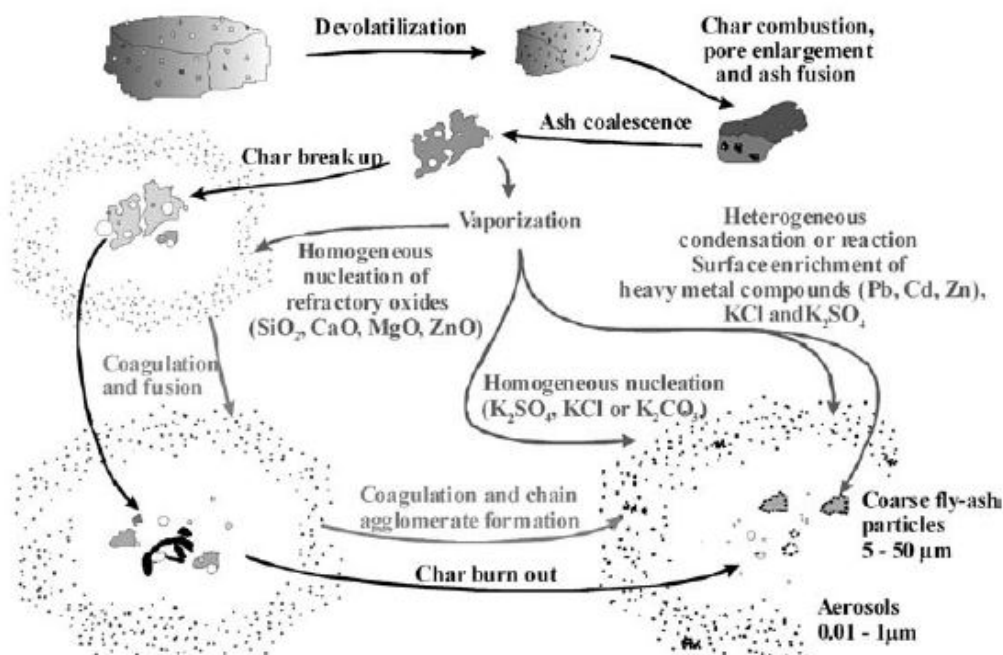

Figure 2.7: Mechanisms involved in ash formation in biomass combustion [Van Loo & Koppejan, 2008]

On one hand, the release mechanisms like vaporization, thermal and chemical disintegration of inorganic matter or organic reactions produce small particles (< 1 µm). The aerosol formed is composed by volatile elements like K and heavy metals (Pb, Cd, Zn) which nucleate and condensate on other particles surfaces or heat exchangers surfaces under supersaturation conditions. On the other hand, residual ash undergo fragmentation, coalescence with other inorganic materials or other chemical or physical transformation which produce larger ash particles (coarse fly-aerosols).

All these transformations depend highly on the conversion technology used. For solid fuel, three different modes of combustion exist:

- Grate combustors,

- Fluidized bed combustors,

- Pulverized fuel combustors.

2.3.1 Grates combustors

In grates combustors, the fuel is distributed on the grate surface which can be static or in motion where the air stream is provided from underneath. The fuel bed is burning on the grate at around 1000-1200 °C with residence time approximatively of 7 minutes.

The figure 2.8 provides an overview of inflows and outflows configurations.
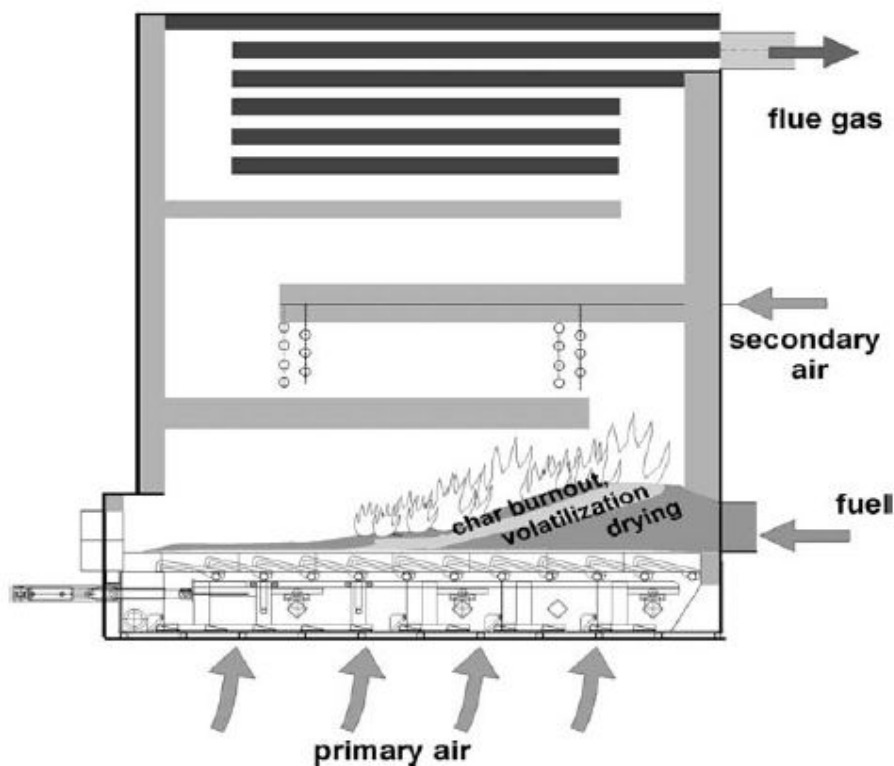
Figure 2.8: Diagram of a horizontally moving grate furnace [Van Loo & Koppejan, 2008]

As we can see in figure 2.9, the combustion produces fly ash and forms aerosols containing volatile elements like alkali metal above the bed. Depending on the local temperatures, sintering or fusion of bed ashes particles can happen. This can lead to the formation of large agglomerates affecting air distribution through the fuel and therefore decreasing ultimately combustion efficiency. Beside these consequences on the combustion, fused ash can make the operations of maintenance difficult.
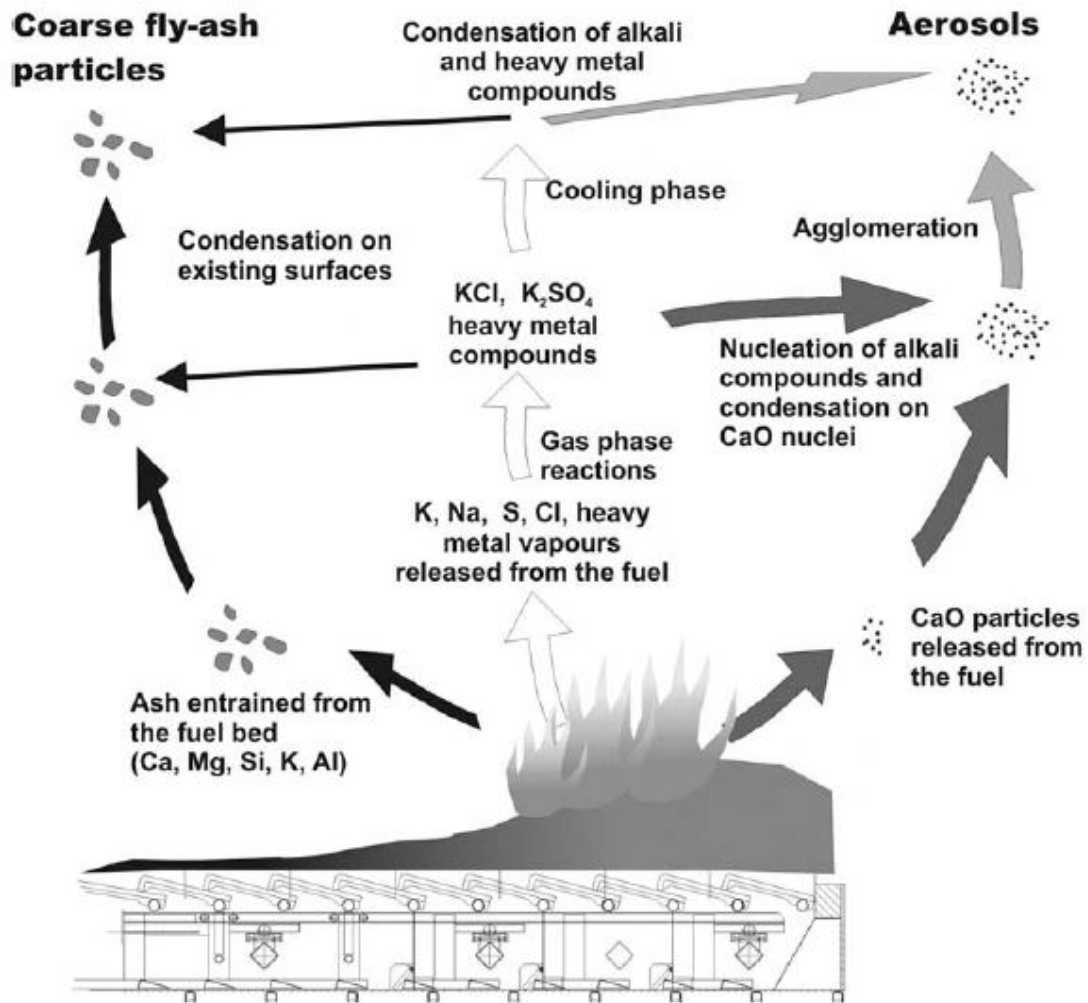

Figure 2.9: Processes involved in fly ash and aerosol release from the combustion of wood on a grate [Van Loo & Koppejan, 2008]

2.3.2 Fluidized bed combustors

Fluidized bed combustion (FBC) is one of the most efficient combustion technology. Thus two types of technologies should be distinguished depending on the configuration of the bed: circulating fluidized beds (CFB) and bubbling fluidized beds (BFB) (see figure 2.10 and figure 2.11)
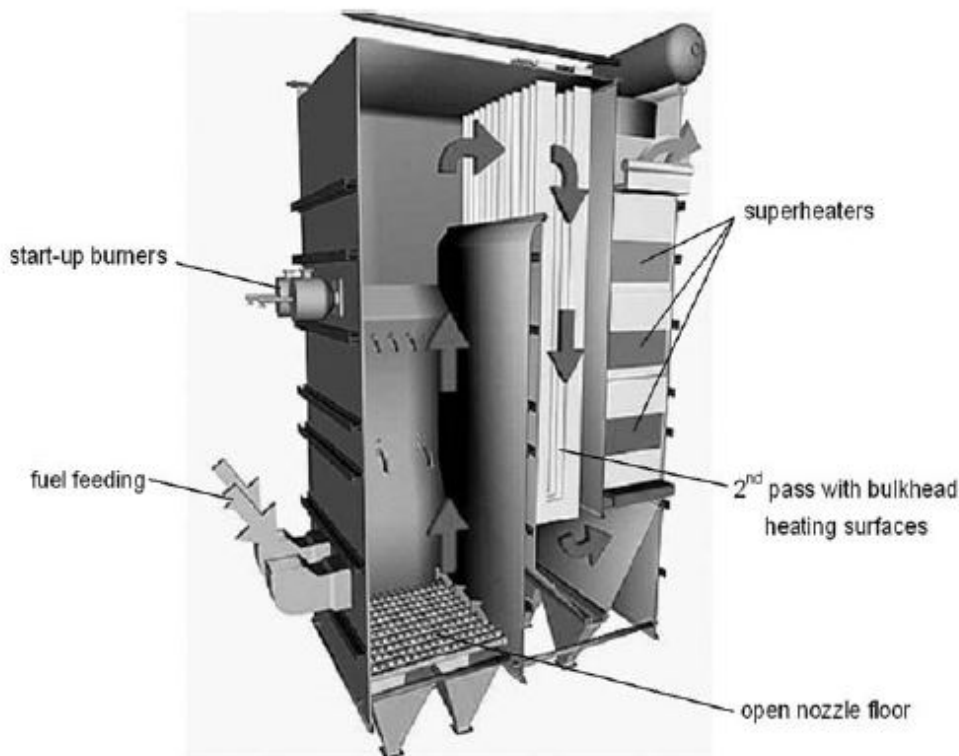

Figure 2.10: BFB furnace [Van Loo & Koppejan, 2008]

In fluidized bed reactors, the particles of fuel are suspended by air steam with coarse-grained bed materials like quartz for example. The combustion temperature tends to be less than 900 °C which leads to lower release of alkali by volatilization and fusion of ashes compared to grate combustors.

In operation, the melting of low-melting point ashes forms low viscosity liquid between bed particles which bond them together. This sintering mechanism causes the particles agglomeration which affect air distribution and eventually the defluidization of the bed obliging operators to remove the bed and replace it.
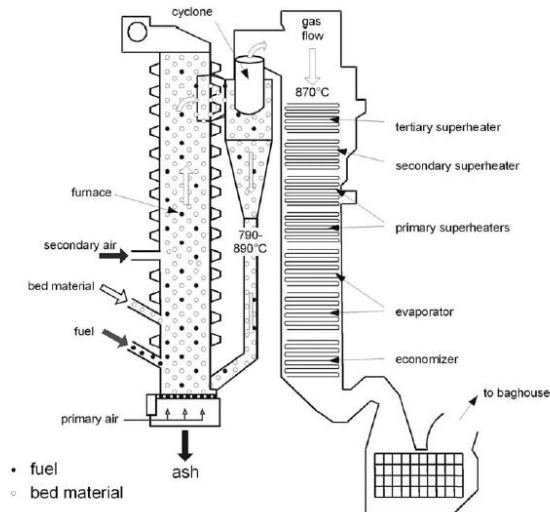
Figure 2.11: CFB furnace [Van Loo & Koppejan, 2008]

One more advanced technology is the Dual Fludized Bed (DFB). This system separates the gasification and the combustion in two different fluidized beds connected together. The figure 2.12 represents the 100 kW dual fluidized bed gasification pilot plant built at the Vienna University of Technology.
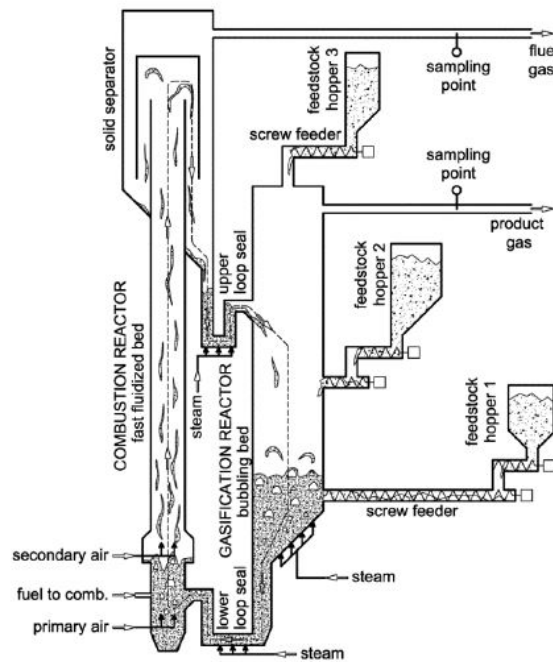
Figure 2.12: DFB gasification pilot plant [Kern et al., 2013]

The feedstock enters the reactor which is a bubbling bed fluidized with steam. The temperature inside the system can rise up to 900 °C.

2.3.3   Pulverized fuel combustors

The pulverized fuel combustors are large boilers used for power generation (see figure 2.13). Compared to other combustion technologies, the flame temperature is very high (around 1600 °C) and residence time is in the range of a few seconds. In this case, biomass is generally co-fired with coal. Therefore, slagging tendency depends highly on the chemisty, especially inorganic compounds, and proportion of both fuels. As biomass has a higher alkali and alkaline earth metals content, slagging propensity increased with the proportion of biomass in the mixture.
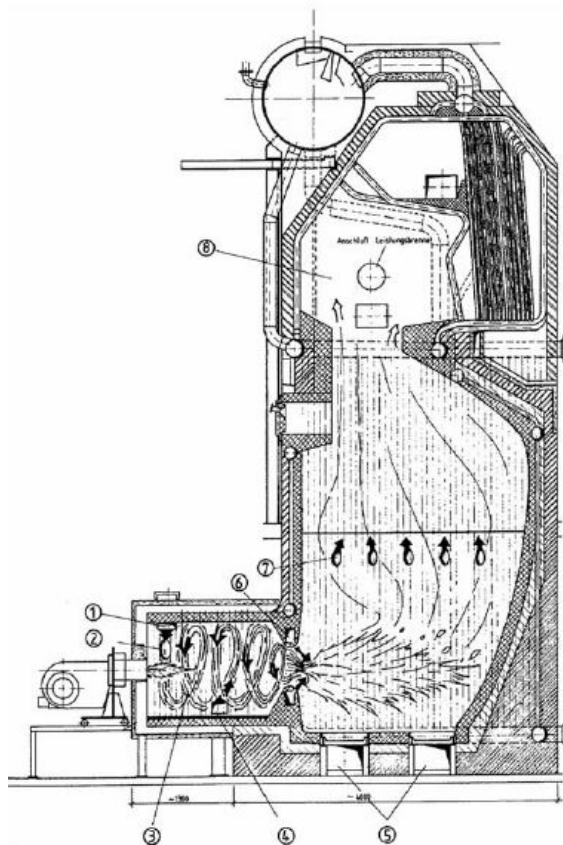

Figure 2.13: Pulverized fuel combustion plant (muffle furnace) in combination with water-tube steam boiler [Van Loo & Koppejan, 2008]
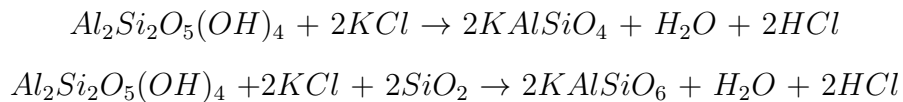
2.4   Current existing solutions

The following solutions have been investigated in the literatur to prevent slagging problem caused by the presence of inorganic components.

2.4.1   Fuel additives

Using additives (or fuel blending) might be a cost-effective solution to tackle the problems mentioned in the section 2.1. The idea is to shift the melting point of ash towards higher temperatures by modifying the chemical composition and therefore reducing bed agglomeration, slagging and corrosion. These combustion additives can be solid, liquid or gaseous. Concretly, additives affect ash composition by increasing the concentration of non-potassium/sodium compounds which cause slagging and sintering problems.

The chemical nature of those additives can be of 5 different types: calcium, phosphorus, sulfur, aluminium and aluminium-silicates. Examples of compounds elevating the melting ash temperatures are alumina oxide (Al_2O_3), calcium oxide (CaO), magnesium oxide (MgO), dolomite ($CaCO_3.MgCO_3$) and kaolin $Al_2Si_2O_5(OH)_4$.

For example, the addition of kaolin mitigate the K evaporation. Indeed, K is adsorbed on kaolin surface before diffusion in the aluminosilicate structure. Potassium then crystallizes in $KAlSiO_4$ (Kalsilite) and $KAlSiO_6$ (Leucite) which have respectively a higher melting point than K-silicate.

$$Al_2Si_2O_5(OH)_4 + 2KCl \rightarrow 2KAlSiO_4 + H_2O + 2HCl$$

$$Al_2Si_2O_5(OH)_4 + 2KCl + 2SiO_2 \rightarrow 2KAlSiO_6 + H_2O + 2HCl$$

2.4.2   Water leaching

Leaching is a pre-treatment technique removing inorganic elements (K, Na, Cl) by submerging biomass in water. By reducing the concentrations of inorganic compounds, the ashes compositions will be affected in a way that their melting temperatures increase.

[Arvelakis et al., 2002] used tap water to remove inorganic elements from olive residue for fluidized bed gasification. Gasification test with leached olive residue demonstrated no

agglomeration problems enabling a longer operation times. The study proved therefore that leaching removed effectively K, Na and Cl. The ash analysis from the same paper is given at the table 2.2.

Table 2.2: Element composition of olive residue ashes given as oxides before and after treatment [Arvelakis et al., 2002]

Ash basis [%]	K_2O	Na_2O	CaO	MgO	SiO_2	Al_2O_3	Fe_2O_3	TiO_2	SO_3	Cl
Untreated olive residue	27,23	4,18	10,21	3,79	32,60	2,95	1,9	0,1	4,97	1,43
Leached olive residue	4,9	0,05	23,38	1,12	43,57	0,62	2,4	0,14	3,29	0,03

2.4.3   Co-firing

Co-firing consists of mixing two different types of fuels in order to reduce economical and operational costs. In our case, the idea is to balance the effects of biofuels having high and low ash melting temperature tendencies by mixing them in order to produce a fuel blend which can be used at higher operational temperatures.

This technic mitigates indeed the impact of low melting ash. However, [Hupa et al., 2017] points out the lack of knowledge regarding fuel blends. Therefore, research are on going to extract the maximum out of this technic.

Chapter 3

Prediction method based on ternary diagrams

Ternary diagrams are mostly used in the literature to classify different types of biomass. However, they can be used as well to predict slagging propensity based on biomass ash composition.

The following chapter will investigate the potential of ternary diagrams as a tool to predict ash melting temperature. Diagrams found in the scientific literature will be described in the context in which they have been utilized. Based on the literature research, advantages and disadvantages will be then discussed.

3.1 Ternary diagrams

3.1.1 Ternary diagram $K_2O - CaO - SiO_2$

[Turn et al., 1997] in his paper, has investigated the efficiency of four different inorganic component removal processes on banagrass feedstock containing a potassium concentration of 1,1%. Treatments were consisting of several processes combination: particle size reduction methods, mechanical dewatering, water rinses and air drying.

Table 3.1: Banagrass treatment processing steps [Turn et al., 1997]

Fuel	Treatment identifica-tion	Size reduction method	Initial dewatering press	Water rinse with secondary dewatering press	Ambient tempera-ture forced air drying
Banagrass	FC-UP	Forage chopper	No	No	Yes
Banagrass	FC-P	Forage chopper	Yes	No	Yes
Banagrass	FC-PRP	Forage chopper	Yes	Yes	Yes
Banagrass	JC-PRP	Jeffco chopper	Yes	Yes	Yes

These treatments were supposed to lower levels of ash, potassium, sodium, magnesium, sulphur and chlorine which was observed for the four of them but not at the same magnitude. Indeed, the alkali indexes calculated for FC-UP, FC-P, FC-PRP and JC-PRP fuel treatments were 0.7, 0.45, 0.23 and 0.11 kg(K_2O+Na_2O)/GJ meaning an improvement in terms of removal efficiency.

The latter results were corroborated by reporting the normalized composition of K_2O, CaO, SiO_2 from each fuel obtained on the following ternary phase diagram (see figure 3.1). As we can see, all the treatments increase the ash melting temperatures by removing inorganic components from left to right. According to the phase diagram predictions based on normalized concentrations, ash melting temperatures for treatments FC-UP and FC-P are inferior to 1000 ℃, FC-PRP and JC-PRP produce ashes with fusion temperature respectively of 1075 ℃ and 1250 ℃. These fusion temperatures are lower than the one from bagasse estimated at 1500 ℃ with the same diagram. In this paper, no comparison with AFT results has been done.
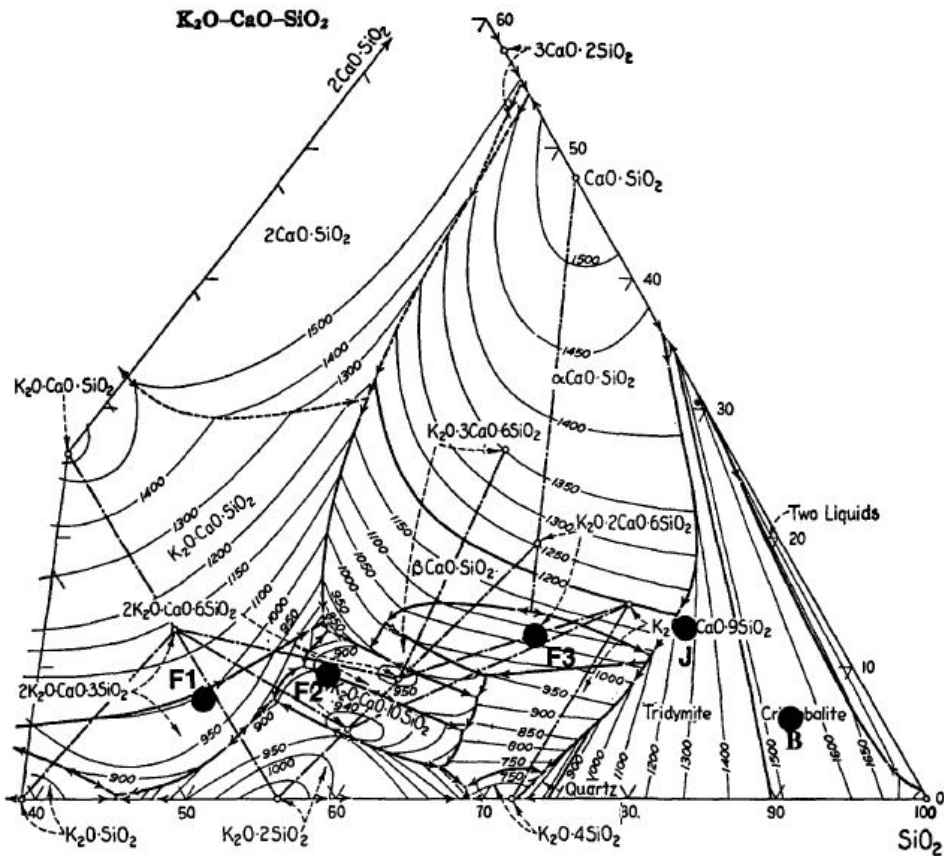
Figure 3.1: Phase diagram of the $K_2O - CaO - SiO_2$ system with location of normalized ash composition of fuel treatments. Label abbreviations: B, bagasse; F1, FC-UP; F2, FC-P; F3, FC-PRP; J, JC-PRP [Turn et al., 1997]

[Jenkins et al., 1996] uses the same phase diagram in the identical context but instead of banagrass, the types of biomass analysed were rice straw and wheat straw which have high slagging tendencies. The ash of the latter were analyzed in terms of composition. Furnace experiments were carried out in order to investigate ash fusibility behaviours. The fuels were ashed at 575 °C and place in a furnace at various temperatures between 575 and 1000 °C . The weight changes, state of fusion and color of the sample were observed and studied. However, no standards procedures were used during the experiments.

The normalized compositions of rice straw (R) and wheat from two different sources (W and Y) were reported in the phase diagram (see figure 3.2).
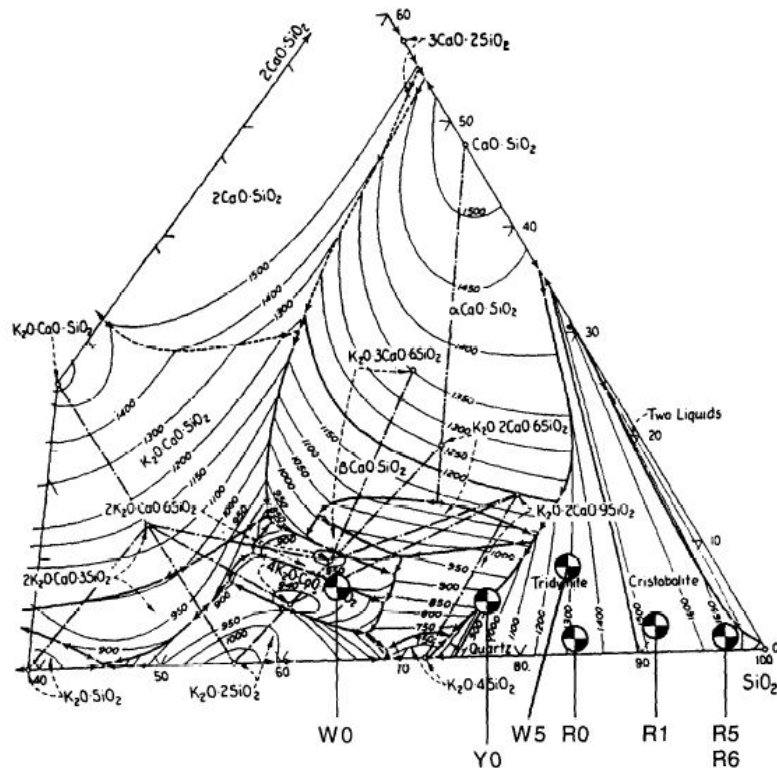
Figure 3.2: Phase diagram of the $K_2O - CaO - SiO_2$ system with location of normalized ash for rice and wheat straw. R=rice, W= wheat straw, Y= wheat straw [Jenkins et al., 1996]

The numbers correspond to the different types of washing treatments in the table 3.2

Table 3.2: Straw washing treatments for rice and wheat straw [Jenkins et al., 1996]

0	Untreated, milled (19 mm), sample not subjected to washing or precipitation
1	Laboratory washed, 100 g whole straw, hand sprayed for 1 min with tap water
5	Laboratory washed, 100 g whole straw, submerged in 7 l distilled water, 24 h
	Rice straw, naturally rain washed:
6	65 mm cumulative precipitation

The same conclusion as previously can be drawn, removing potassium, sodium and chlorine with water increased the ash fusion temperatures. Most importantly, the temperatures predicted by the ternary diagram are in accordance with furnace experiments.

[Öhman et al., 1999] studied the possibility to prevent bed agglomeration in fluidized bed for the combustion of wheat straw and bark by adding kaolin. The experiments were performed in a bench-scale fludized bed reactor (5 kW). The material used for the experiment is normal quartz sand sieved to a particle size between 200 and 250 μm.

The bed temperature was maintained at 760 °C and the melting behaviour of bed coating was analysed. The different melting profiles were obtained thanks to a procedure defined in the same paper (see figure 3.3). The different curves correspond to several melting measurement points on the coating and the broken lines represent the initial bed agglomeration which shifts to higher temperatures with kaolin addition.
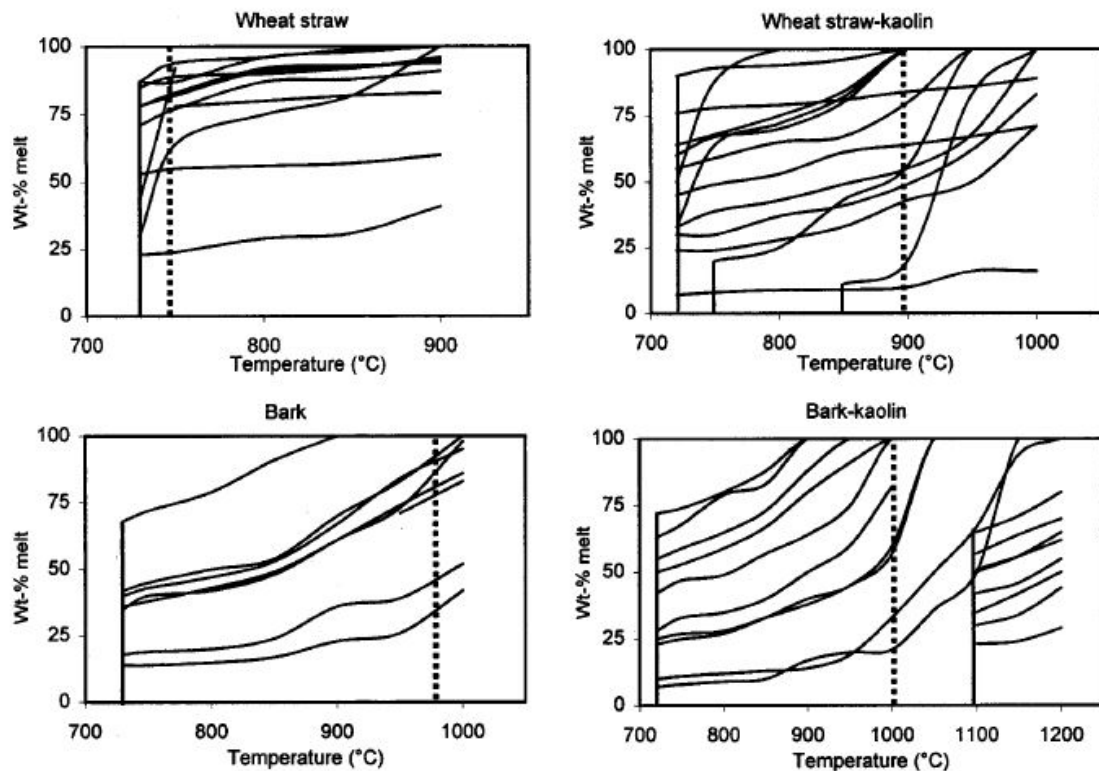
Figure 3.3: Melting behaviours of various spot characteristics of bed coatings from different bed samples (solidus line) [Öhman et al., 1999]

As the main composition of bed particles coatings is $K_2O - CaO - SiO_2$ ($> 90\%$). The following phase diagram (see figure 3.4) was used. The plot marks for the different bed particles coating responsible for agglomeration are: bark (un-filled triangles), bark-kaolin (filled triangles), wheat straw (un-filled squares), wheat straw-kaolin (filled squares).
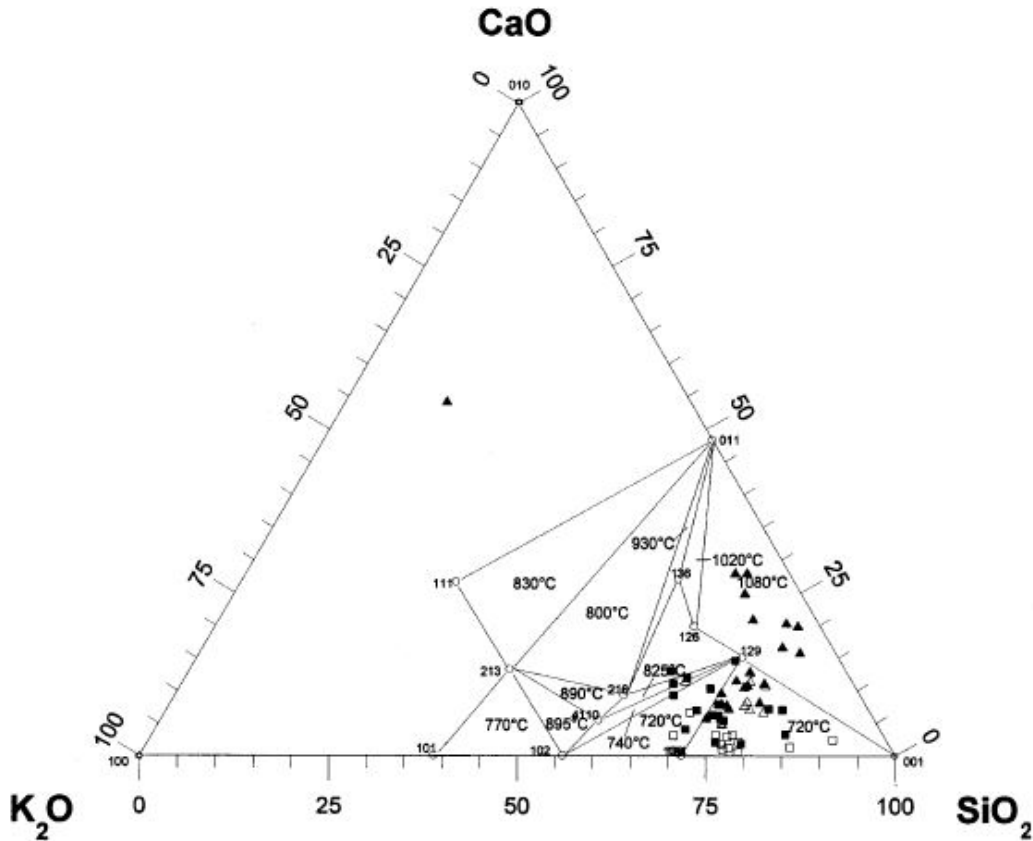

Figure 3.4: Ternary diagram $K_2O - CaO - SiO_2$ [Öhman et al., 1999]

Most of coating compositions are located in the SiO_2 corner as expected. The initial agglomeration temperatures for wheat straw and bark are 739 and 998 °C respectively. This temperature rises to 886 and 1000 °C when kaolin is added corroborating the results obtained in figure 3.3 (dotted lines).

3.1.2 Ternary diagram $K_2O - Al_2O_3 - SiO_2$

[Nording et al., 1994] proposed to classify fuels according to their ashes Si, K and Al content given as oxides (% of ash). Data of 15 biofuels and types of coals have been compiled from different databases (see table 3.3).

Table 3.3: Element composition of olive ashes given in oxides [Nording et al., 1994]

Fuel group	Si(%)	Al(%)	Fe(%)	Mg(%)	Ca(%)	K(%)	Na(%)	P(%)
Wood	0,0028	0,0019	0,0026	0,016	0,065	0,04	0,018	0,0075
Debris	0,5	0,11	0,047	0,051	0,42	0,16	0,021	0,043
Bark	0,14	0,033	0,019	0,062	0,6	0,17	0,036	0,041
Needles	-	-	0,0056	0,078	0,3	0,51	-	0,15
Salix	0,038	0,0055	0,0067	0,056	0,37	0,31	0,011	0,076
Timothy	1,4	0,032	0,024	0,13	0,58	2,2	0,056	0,13
Lucerne	0,15	0,019	0,022	0,18	1,6	2,5	0,092	0,29
Rape	2,1	0,22	0,16	0,1	1,3	1,0	0,14	0,085
Barley	1,2	0,037	0,026	0,1	0,4	1,1	0,2	0,092
Wheat	1,8	0,023	0,026	0,11	0,4	0,94	0,042	0,075
RC summer	1,6	0,019	0,016	0,13	0,38	1,1	0,091	0,18
RC spring	4,6	0,11	0,06	0,05	0,2	0,34	0,068	0,1
Peat Ref	0,52	0,28	0,63	0,086	0,89	0,02	0,014	0,04
Peat average	0,55	0,24	0,67	0,064	0,38	0,025	0,0092	0,068
MSW	0,28	0,88	4,0	0,12	4,57	0,17	0,21	2,0
Coal 1	3,4	0,88	0,22	0,052	0,27	0,058	0,087	0,015
Coal 2	4,8	2	0,47	0,13	0,38	0,15	0,11	0,02

The K_2O, Al_2O_3 and SiO_2 compositions were reported in the following ternary diagram. The liquidus temperature shows the problematic zone regarding deposit formation and bed sintering with a comparison with coal (see figure 3.5).
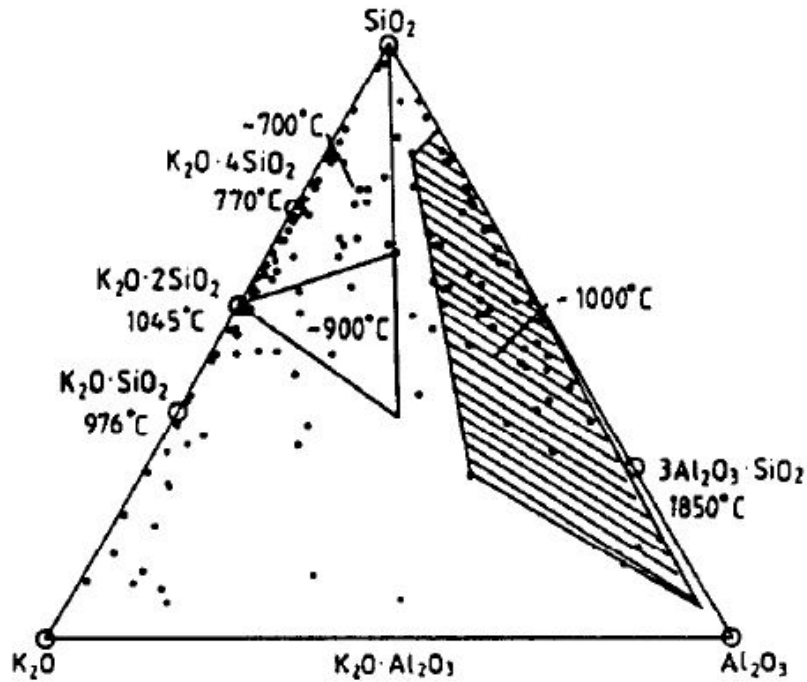
Figure 3.5: $K_2O - Al_2O_3 - SiO_2$ ternary diagram with some liquidus temperatures and the compositions of biomass fuels (bullets) and coals (in hatched area) [Nording et al., 1994]

[Skrifvars et al., 1999] studied the influence of co-firing on ash melting behaviour in a pulverized coal-fired (PF) boiler running with coal and straw. Three sets of fly ash and bottom ash corresponding to three different energy shares of straw to the overall mixture straw-coal have been sampled (see table 3.4).

Table 3.4: Straw and coal shares on energy basis for different experiments [Skrifvars et al., 1999]

Experiment n°	3	4	5
Straw [%]	20	10	0
Coal [%]	80	90	100

Table 3.5: Standard ash fusion test results and comparison to melting curves [Skrifvars et al., 1999]

	IDT-AFT(℃)	%melt	IDT-STA(℃)	HT (℃)	%melt	FT(℃)
MKS3FA	1180	36.4	1038	1290	65.1	1500
MKS4FA	1190	1.1	1171	1330	43.3	1490
MKS5FA	1220	2.5	1185	1430	-	1490
MKS3BA	1150	10.7	1042	1270	49.1	1490
MKS4BA	1150	4.3	997	1280	38.6	1460
MKS5BA	1150	11.0	992	1300	54.2	1410

As table 3.5 shows, the initial deformation temperature (IDT) slightly decreases when straw share increases due its high slagging tendency. However, there is a non-negligible gap between STA and AFT measurements. The reason is that STA detects melting formation well below the AFT. $K_2O - Al_2O_3 - SiO_2$ ternary diagram has been used to estimate melting behaviour of the bottom and fly ashes in figure 3.6 .
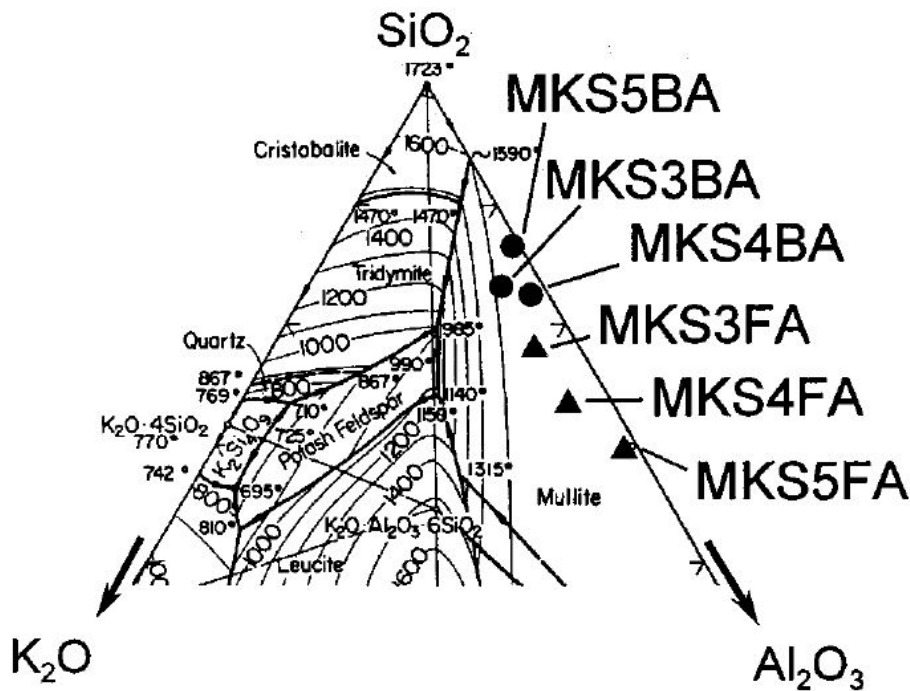
Figure 3.6: Chemical composition of fly and bottom ash illustrated in $K_2O - Al_2O_3 - SiO_2$ ternary diagram [Skrifvars et al., 1999]

The K_2O, Al_2O_3 and SiO_2 concentrations have been normalized to 100% for both type of ashes. One limit is that Fe_2O_3, CaO, MgO concentrations have been neglected in both cases although they contribute to decrease the melting temperature.

However, it seems that the melting temperature measured by STA (1038 ℃) for MKS3FA seems to fit with the one predicted by the above phase diagram (985° C) which can not be said for the other flying ash. According to the diagram, the melting should be completed above 1500 ℃ for the three fly ashes which seems to be in accordance with measurements. Regarding the bottom ashes, the diagram predicts a melting point around 985 ℃ and a completed melting at above 1600 ℃ which is way higher than what was measured. This might be due to the fact that the Fe_2O_3, CaO ash contents have been neglected.

3.2 Pseudo-ternary diagrams

3.2.1 Ternary diagram $CaO(+MgO) - K_2O(+Na_2O) - P_2O_5$

[Grimm, 2012] reported compositions of sieved bed ash particles for each fuel/fuel mixture used in a $CaO(+MgO) - K_2O(+Na_2O) - P_2O_5$ pseudo-ternary diagram to better understand bed agglomeration. For each fuel/fuel mixture, the total proportion of K_2O, Na_2O, CaO, MgO and P_2O_5 was determined (see table 3.6).

Table 3.6: Sum of the oxides (given in wt%) in the sieved bed ash (sand minerals excluded) DDGS: Wheat distillers dried grain with solubles; PA: Phosphoric acid [Grimm, 2012]

		$K_2O+Na_2O+CaO+MgO+P_2O_5$
A	DDGS	89,4
B	Rapeseed meal	91,7
C	40 wt% DDGS in Logging residues	84,6
D	50 wt% DDGS in Willow	86,7
E	30 wt% Rapessed meal in bark	81,3
F	Logging residues +PA(low)	85,0
G	Logging residues +PA (high)	82,0
H	Wheat straw 2 + PA (low)	78,0
I	Wheat straw 2 + PA (medium)	78,5
J	Wheat straw 2 + PA (high)	72,3

The different weight percentages were then reported in the following ternary diagram (see figure 3.7).
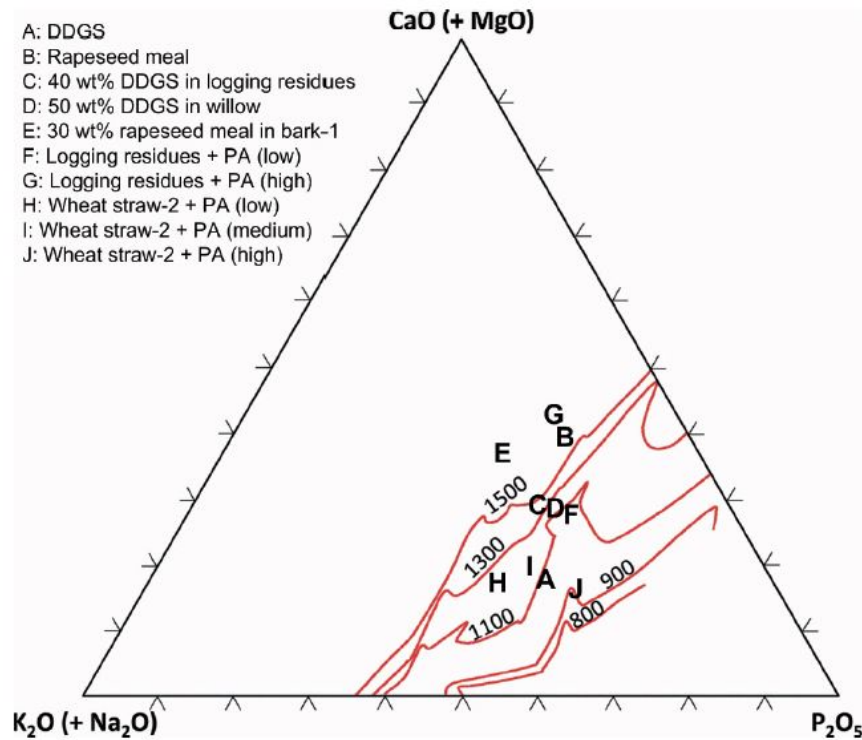
Figure 3.7: Sum of the oxides (given in wt%) in the sieved bed ash (sand minerals excluded) [Grimm, 2012]

The use of such diagram enables the experimenter to predict the nature and chemical composition around the temperature at which the combustion is taking place. Indeed, all ash compositions closed to the binary $K_2O - P_2O_5$ (40-60 wt% K_2O) reveal the formation of low melting compounds down to 590°C. The diagram enables as well the identification of differences in terms of fuels behaviours containing high concentration of Ca and Mg. On one hand, high Ca concentrated fuels tend to form unproblematic phosphates $CaK_2P_2O_7$ (e.g. rapeseed meal) and on the other hand, high Mg concentrated fuels form low melting point compounds $K_2MgP_2O_7$ (e.g. DDGS) explaining agglomeration tendency discrepancies between the two elements. The author conclusion mentioned that the melting temperature predicted by such phase diagrams are higher than the real values during the phosporus-rich fuel combustions. The reason is related again to the negligence of other components than the ones considered in the diagram.

3.2.2 Complex ternary diagram

[Vassilev et al.,2014] reported 55 types of biomass ash compositions in the following pseudo-ternary diagram taking into account more oxides (see figures 3.8 and 3.9).
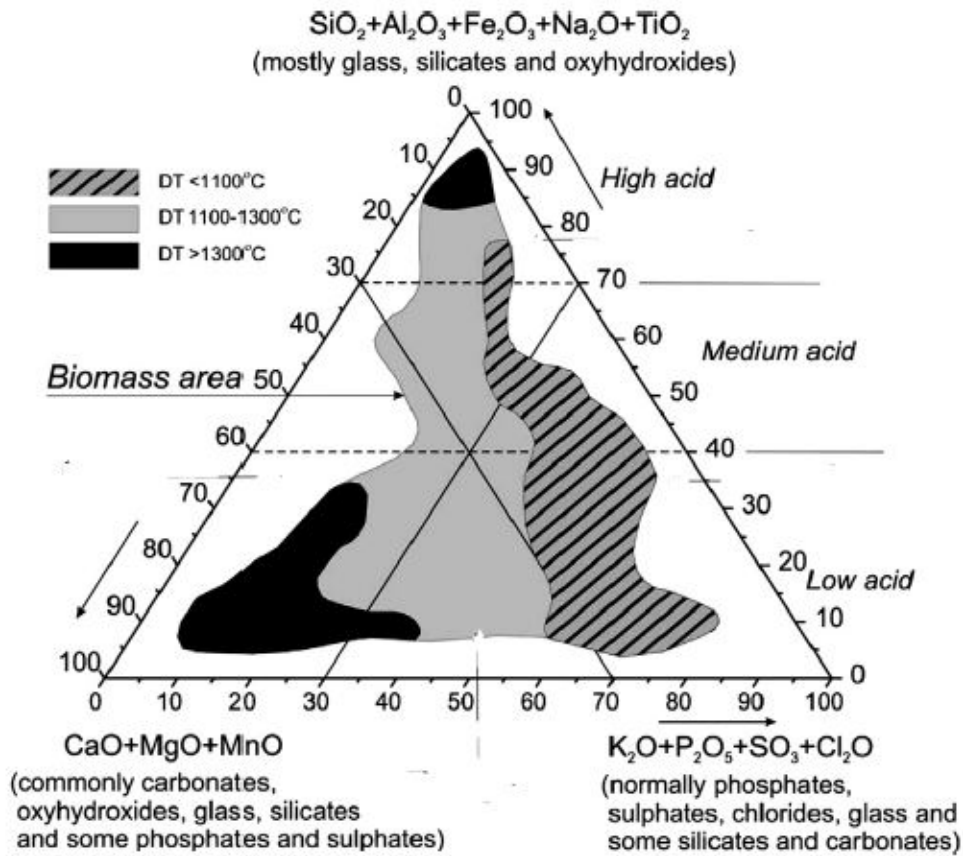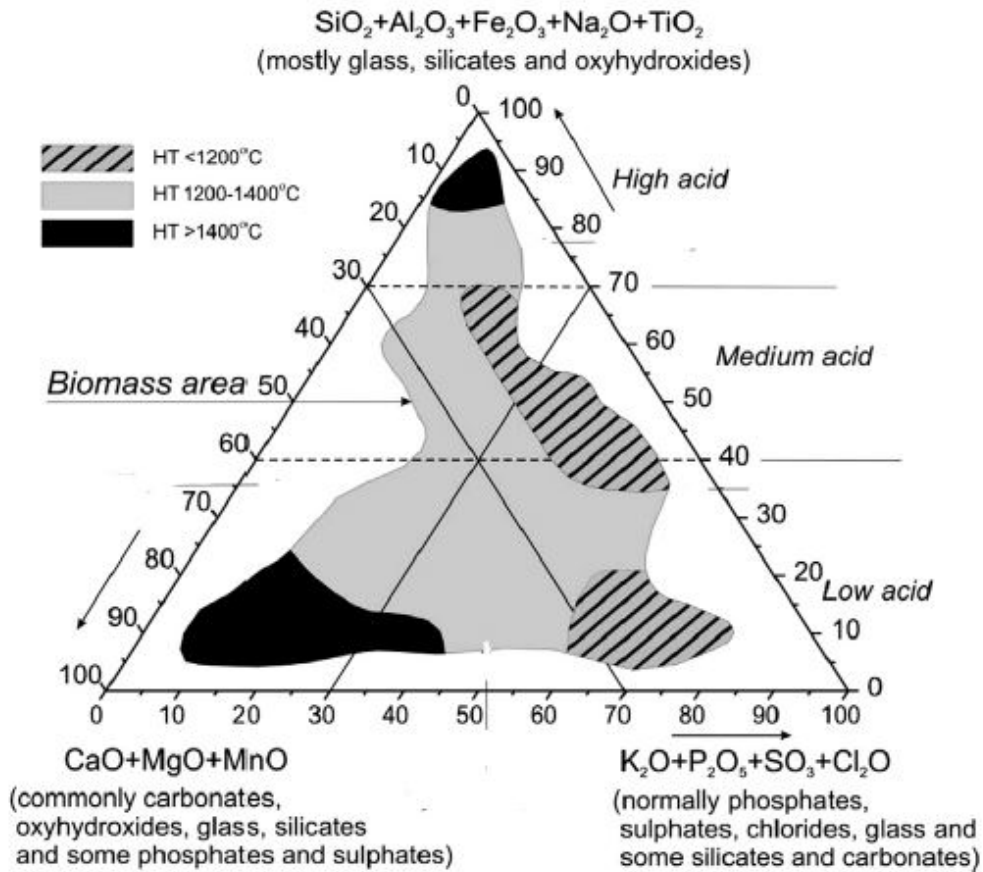

Figure 3.8: Areas of low (<1100°C), medium (1100-1300°C) and high (>1300 °C) initial deformation (DT) temperatures for 55 varieties of biomass in the chemical system of biomass ash, wt.%. Adapted from [Vassilev et al., 2014]

This classification in the diagram reveals the presence of three different important areas for deformation temperature:

- low deformation temperature DT < 1100 °C,

- medium deformation temperature DT 1100-1300 °C,

- high deformation temperature DT > 1300 °C.

Another classification for hemispherical temperature has been proposed in the same paper:

Figure 3.9: Areas of low (<1200°C), medium (1200-1400°C) and high (>1400 °C) initial hemispherical (HT) temperatures for 55 varieties of biomass in the chemical system of biomass ash, wt.%. Adapted from [Vassilev et al., 2014]

- low hemispherical temperature HT < 1200 °C,

- medium hemispherical temperature HT 1200-1400 °C,

- high hemispherical temperature HT > 1400 °C.

3.3 Advantages and disadvantages of ternary diagrams

The ternary diagrams are a powerful thermodynamic tool for decision-making because the melting temperature and different phases are given as function of the composition. Thanks to them, no experimental system has to be built reducing considerably costs. However, the main limitation is the composition approximation made when other compounds beside the three components considered are neglected. This approximation can have a huge impact on results accuracy in a multi-component mixture like biomass ash. Considering a simplified ash composition by normalizing can poorly predict ash melting temperature and therefore lead to wrong decision-making.

[Grimm, 2012] mentioned that the ash particles considered are projections in the ternary systems. Better predictions might be obtained by considering a quaternary system $K_2O(Na_2O) - CaO - P_2O_5$ assuming that K and Na have the same behaviours. However, using those systems (ternary-quaternary) would suppose that the concentration of Si is negligible which is not the case in that study because of the presence of a non-negligible SiO_2 amount. Therefore, the author encouraged to study interactions in silicate and phosphate systems.

Nevertheless, ternary diagrams can be interesting if the sum of the three components considered in the ternary systems contribute to minimum 90% of the overall composition. The usage of pseudo-diagram like figure 3.8 has a certain potential as well because they reduce the approximation made by taking into account more components which leads to better predictions.

Chapter 4

Practical part

The combustion of an olive pellet feedstock has been performed in a lab-scale fluidized bed reactor provided by the Institute of Chemical, Environmental and Bioscience Engineering at TU Wien. A duplicate determination of ashes melting point has been carried out in order to check the consistency of the results. The outputs of the experiments are compared to the results obtained by AFT or predicted by ternary diagrams in the literature.

First, the material and equipment used during the experience are described. In a second step, the outputs of the experiments regarding temperatures and pressures drop measured are underlined and described in order to draw conclusions. Finally, future considerations regarding potential research work are envisaged.

4.1   Material and equipment

4.1.1   Feedstock

The feedstock used for the experience is olive pellet residue (see figure 4.1). In order to estimate the quantity and the composition of ashes produced during thermochemical conversion, feedstock ashes have been analysed. The elemental composition olive ashes as element and oxides was analyzed using XRF spectroscopy by the Institute of Chemical Technologies and Analytics at TU Wien (see tables 4.1 and 4.2). The methodology carried out for the analysis are DIN standards.

Figure 4.1: Olive pellet feedstock used for FBC

Table 4.1: Analysis data of olive ash [Kohl et al., 2014]

		Olive Residue
Ashes (550 ℃)	wt%	4,6
C	wt% (db)	49,3
H	wt% (db)	5,8
N	wt% (db)	1,0
S	wt% (db)	0,1
Cl	wt% (db)	0,1
Volatile	wt% (db)	75,8
Crucible coke	wt% (db)	24,2
Higher heating value	kJ/kg	20268
Calorific value	kJ/kg	18983
Ash fusion test		
Deformation temperature	℃	840
Hemispherical temperature	℃	not reported
Half hemisphere temperature	℃	not reported
Flow temperature	℃	1440

Table 4.2: Element composition of olive ashes given as oxides [Kohl et al., 2014]

Oxide	wt%
SnO	0,04%
MoO_3	0,02%
Nb_2O_5	< 0,01%
ZrO_2	0,01%
SrO	< 0,01%
PbO	< 0,01%
As_2O_3	< 0,01%
ZnO	0,07%
CuO	0,57%
NiO	0,19%
Co_3O_4	0,41%
Fe_2O_3	1,19%
MnO	0,04%
Cr_2O_3	0,53%
V_2O_5	<0,01%
TiO_2	0,08%
CaO	11,86%
K_2O	42,51%
Cl	3,54%
SO_3	5,28%
P_2O_5	8,07%
SiO_2	12,92%
Al_2O_3	2,47%
MgO	6,08%
Na_2O	4,12%

4.1.2   Bed material

The material used as bed for fluidized-bed experiments is quartz (see figure 4.2). The size is one important parameter to ensure the bubbling properties of the bed. The granulometry used corresponds to a Sauter diameter d_{sv} of 0,299 mm. The quartz particles were therefore sieved to isolate the size range [400;500] μm.

Figure 4.2: Quartz particle used for the experiments

4.1.3 Fluidized bed reactor

The fluidized bed used for the experiments has been designed and built at TU Wien. The operational parameters were postulated as mentioned in [Eßletzbichler, 2017]. As figure 4.3 shows, the FBC systems is composed of the following individual part:

1. Fuel bunker: vessel in which fuel pellets are stored. Biomass pellets can be inserted or removed by taking off the bunker cover plate. The pressure of nitrogen inside is adjusted in order to unable the hot flue gas to go in and therefore avoiding inflammation of the fuel,

2. Feeding screw: system used to convey biomass pellet above the reactor. The feed flowrate is a function of the speed at which the screw is rotating. The latter can be adjusted by changing the frequency at which the motor is functioning,

3. Sparger plate: the air used to fluidize the bed is entering the reactor through a sparger plate of 31 holes of 1 mm diameter ensuring a high air velocity,

4. Combustion area: combustion is occurring in a steel tube of 53,1 mm diameter and 335 mm height (lab-scale system). In this area of the system, thermal conversion of biomass and ash production occurs,

5. Air Inlet: air flowrate can be adjusted by rotameter and valves. The latter is preheated before entering the combustion zone.

Process control is also an important part of the system enabling measurements. Different sensors (temperatures, pressures and emissions) are integrated in this experimental system:
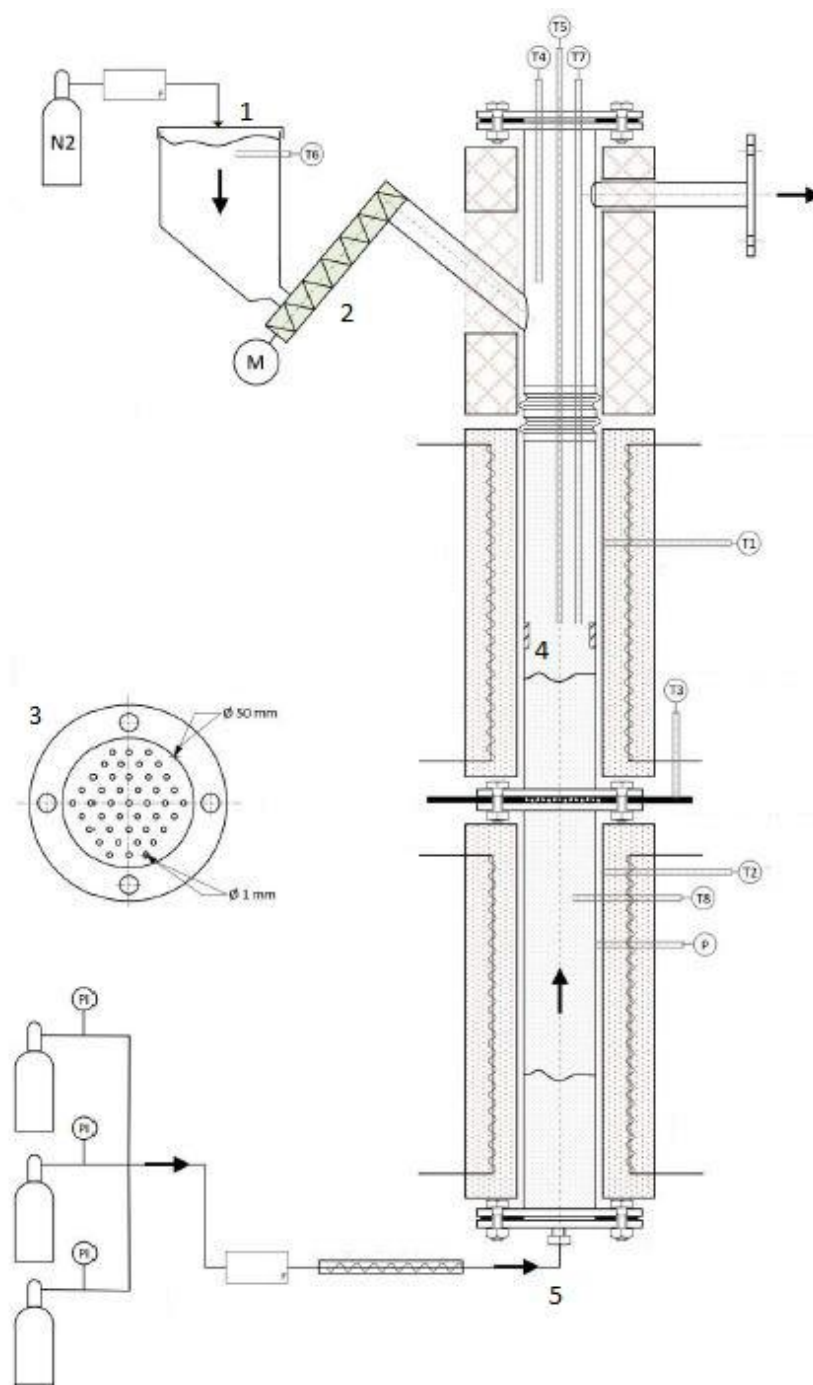
Figure 4.3: Lab-scale fluidized bed reactor at TU Wien adapted from [Eßletzbichler, 2017]

T1: Temperature sensor for the upper heating shell,

T2: Temperature sensor for the lower heating shell,

T3: Temperature sensor for the flange and the sparger plate,

T4: Not used,

T5: Temperature sensor for the combustion zone,

T6: Temperature sensor for the fuel bunker,

T8: Temperature of preheating,

P: Pressure sensore under sparger plate.

The flue gas is cooled down before being analyzed. The composition of the fluegas is as well controlled to monitor the quality of the combustion thanks to a paragmagnetic, TCP and IR for CO_2, CO, CH_4, H_2 and O_2 analysator (see figure 4.4).
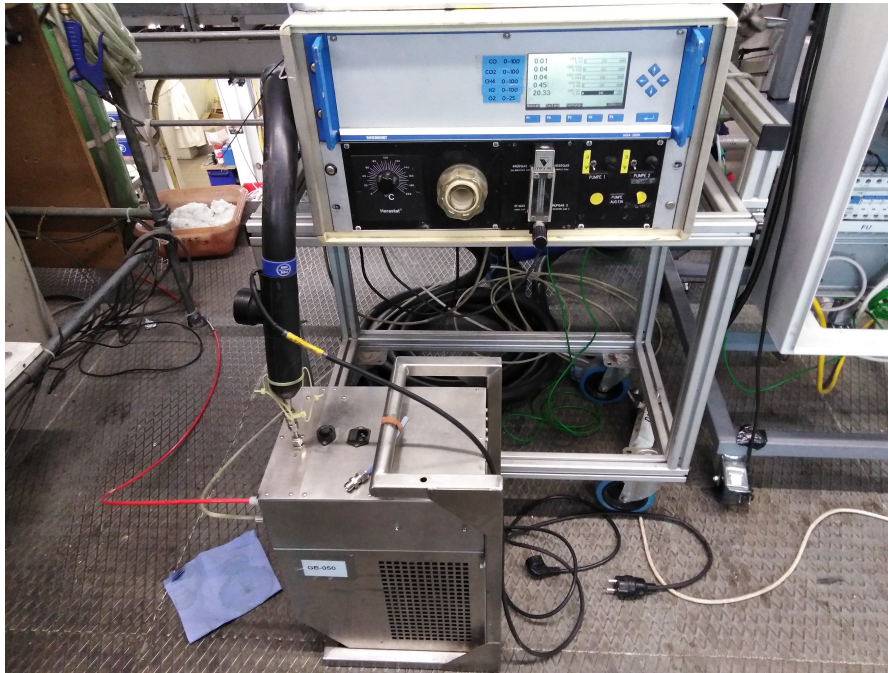
Figure 4.4: Rosemount multicomponents analysator NGA 2000

4.2   Results and discussions

4.2.1   Feedscrew calibration curve

In order to identify the fuel quantity introduced into the reactor, the feedscrew was calibrated by measuring pellets flowrates at three different motor frequencies (see table 4.3 and figure 4.5). Each flowrate is determined by measuring the quantity of fuel provided by the screw during a time period of 15 minutes.

Frequency (Hz)	Flowrate (g/h)
15	67
25	101
50	175

Table 4.3: Measurement points for feedscrew calibration curve
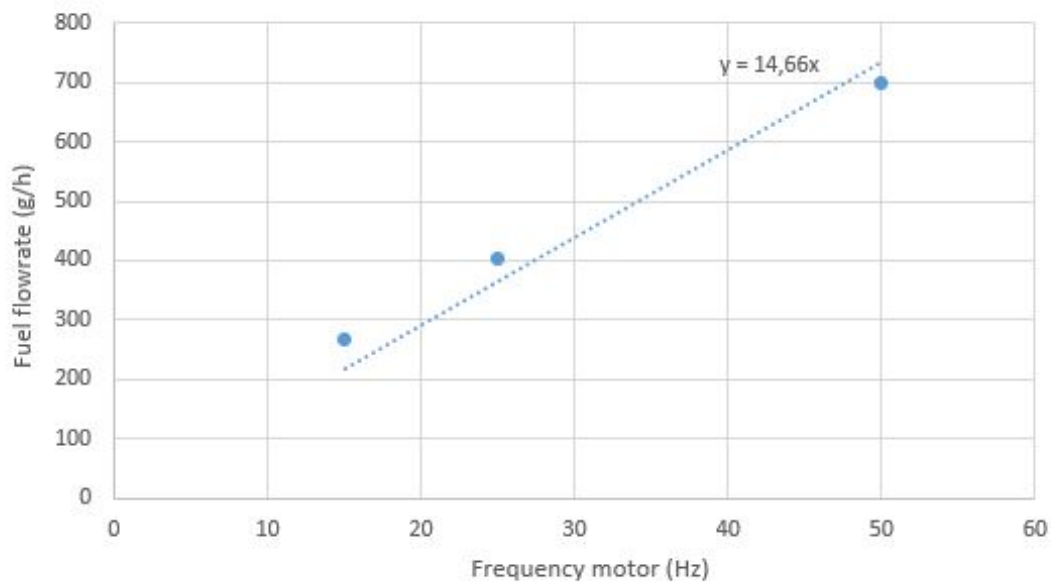
Figure 4.5: Calibration curve used for experiments

4.2.2 Experimental procedure

A summary of the operating conditions during both experiments are given in table 4.4

	Experiment 1/2
Frequency (Hz)	10
Pellets flowrate (g/h)	147
Quartz mass (g)	350
$d_{sv}(mm)$	0,299
Air flowrate (Nl/min)	16

Table 4.4: Operation parameters for the experiments performed in fluidized-bed reactor

The bed temperature is progressively brought to 950-960 °C for both experiments (see figures 4.6 and 4.7). The air flowrate was fixed to 16 Nl/min in order to create appropriate fluidization conditions and to provide enough oxygen for complete combustion. Before introducing the fuel into the reactor, the reactor as well as the bed is heated progressively to 635 °C to avoid thermal stress thanks to the heating shells. Afterwards, the fuel was introduced at a rate 147 g/h.

During the run, temperatures, pressure mentioned in the figure 4.3 are recorded every 5 seconds. The total time between the beginning of fuel feeding and bed agglomeration time is recorded as well. The total time from the beginning of the fuel feeding and agglomeration were 5 hours for the first experiment and 2,2 hours for the second experiment. After the bed agglomeration occured, the installation is cooled down and the agglomerated bed is removed and the agglomerates are sieved for separation.

The following temperature profiles before agglomeration have been measured during both experiences. From 635 °C, the temperature increases till a maximum of 950-960 °C (see figures 4.6 and 4.7). This increase is explained by the heat released by the fuel during the combustion and an increase of heating shells temperature as the heating value of olive pellets is not enough to reach that maximum. The bed agglomeration occured when a sudden change in temperature and pressure profiles are observed.
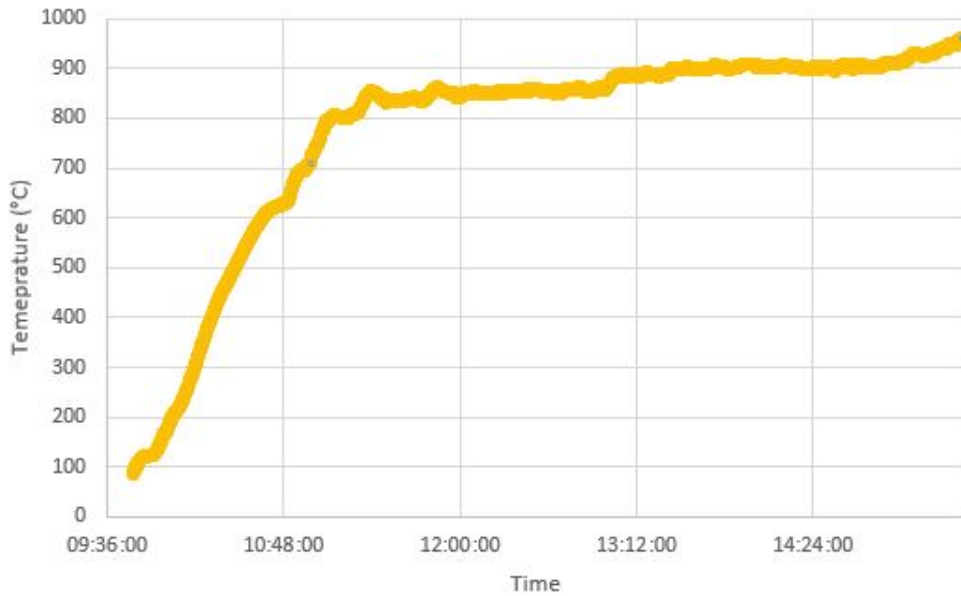
Figure 4.6: Heating profile-Experiment 1
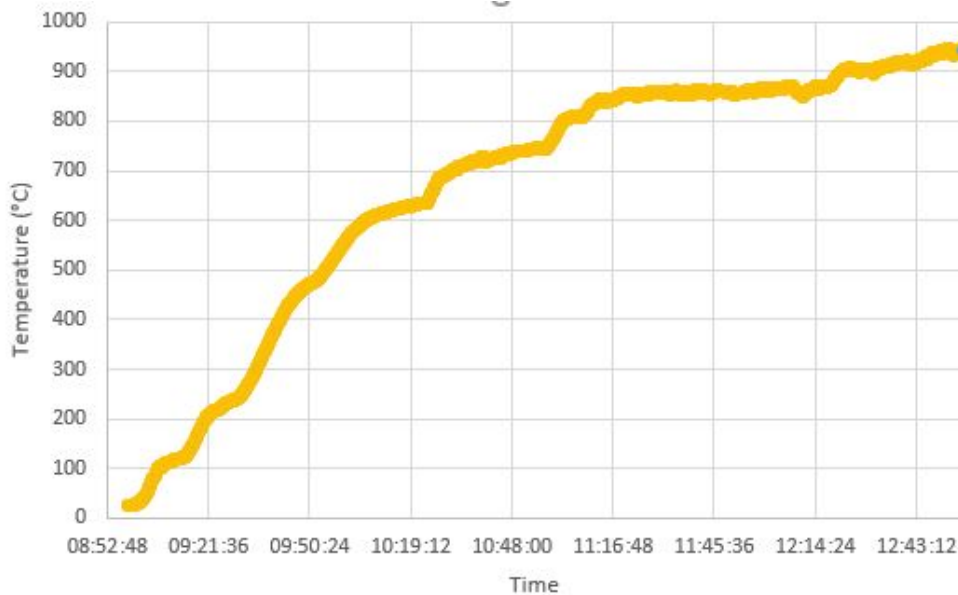
Figure 4.7: Heating profile-Experiment 2

4.2.3 Temperatures and pressures profiles

As the bed temperature stabilized around 960°C, the latter progressively drops shown by the black lines (see figures 4.8 and 4.9). As the ashes progressively build and melt in the bed, the particles of quartz sinter together disturbing the bubbling behaviour of the bed. As a consequence, the temperature measured in the bed is decreasing because of a

lower combustion efficiency. The table 4.5 gives the exact combination of temperature-pressure for both experiments at the inflexion points.
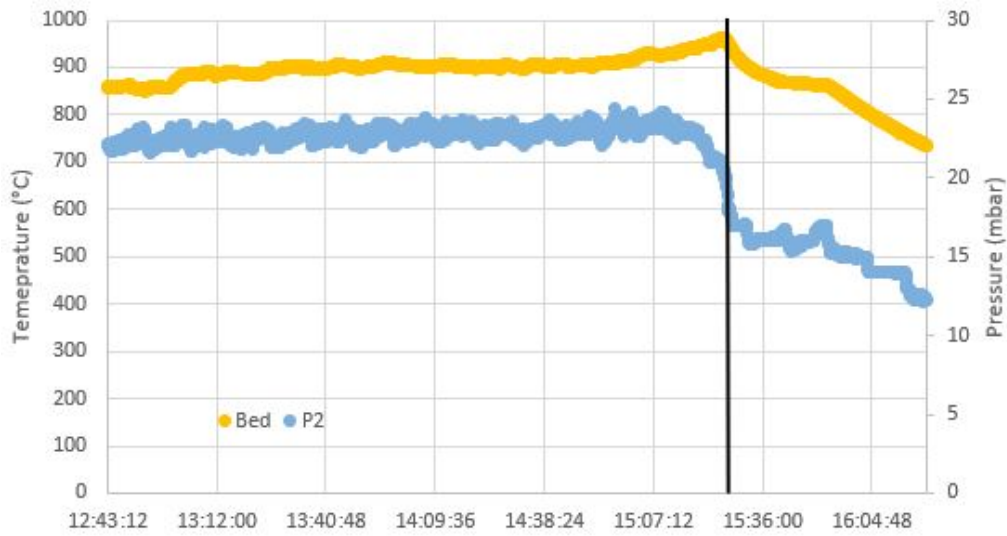
Figure 4.8: Changes in temperature and pressure-Experiment 1
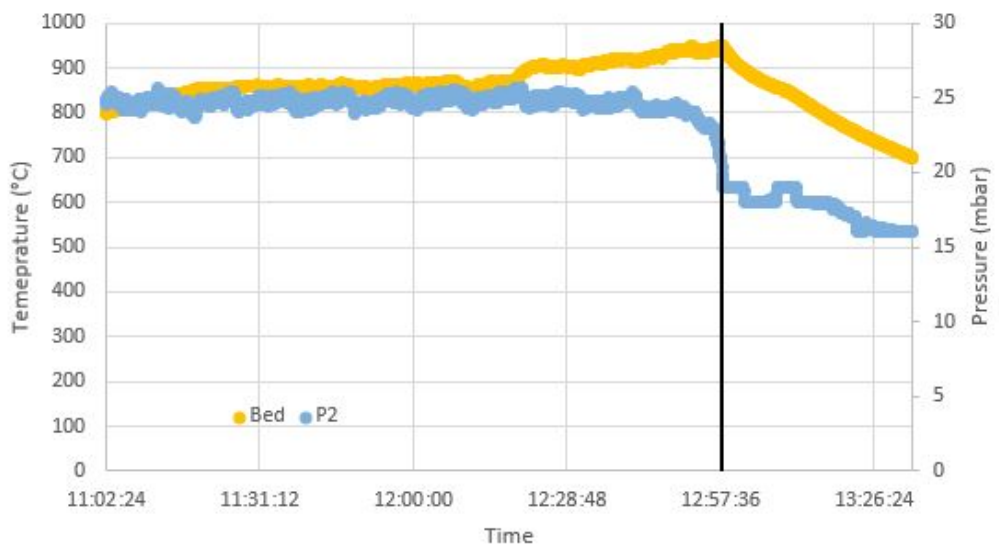
Figure 4.9: Changes in temperature and pressure-Experiment 2

Table 4.5: Temperature and pressure at inflexion points for both experiments

	Experiment 1	Experiment 2
Temperature (°C)	955,6	948,4
Pressure (mbar)	19,5	20,3

This observation is corroborated by the pressure drop. Indeed, as the ash melt, the agglomerates become bigger and bigger offering a higher counter-pressure to the air flowrate and therefore, explaining the decrease of the pressure under the bed.

4.2.4 Analysis of produced ash

The agglomerates formed during the combustion are shown in the figures 4.10 and 4.11.

Figure 4.10: Agglomerates in bed-Experience 1

Based on the fuel flowrate and time interval between the beginning and the end of fuel load, theoretical ash content in the bed can be calculated.

For the first experience, 735 g of olive pellets were introduced in 5 hours giving 34 g of ashes considering an ash content of 4,6% (see table 4.1). If this amount of ash is summed to the bed mass (350 g), a total of 384 g is obtained. Experimentally, a total amount (bed and ash) of 428 g was measured meaning a difference of 44 g between predicted and experimental values. This can be explained by several factors: presence of tinder (metal oxides) from the reactor tubewalls, weight measurements errors of the balance, loss of materials during sampling, errors related to the determination of the calibration curve.

For the second experience, 328 g of olive pellets were injected in 2,2 hours which gives 15 g of ash considering an ash content of 4,6% (see table 4.1). If this amount of ash is summed to the bed mass (350 g), we obtained a total of 365 g. Experimentally, a

Figure 4.11: Agglomerates in bed-Experience 2

total amount (bed and ash) of 385 g meaning a difference of 20 g between predicted and experimental values. The reasons are the same as the ones mentioned in the previous paragraph.

The excess between theoretical and experimental values is more or less divided by two between first and second attempt. The main reason of this difference is related to the time of the second experience which is more or less half of the time of the first attempt. This means that if the experiment time would have been equal, the amount of ash produced in both experiments would have been similar. Furthermore, regarding the second experiment, 5% of ash content is enough to agglomerate the bed too in comparison to 10% of ash content in the first experiment.

As far the melting behaviour prediction is concerned, the temperature at which the agglomeration occured is about 950 °C which is between 840 °C, the deformation temperature and 1440 °C, the flow temperature provided by the ash fusion test in table 4.1. At 840 °C the ash begins to melt but the quantity of fused material is not enough to agglomerate the bed.

4.3 Comparison with literature

In [Scala et al., 2006], the fluidized bed combustion of olive residue was investigated in a bench-scale reactor. The properties of olive husk used in the experiment is given at the Table 4.6.

Table 4.6: Properties of Olive Husk [Scala et al., 2006]

	exhausted husk	virgin husk
Proximate analysis (wt%)		
Moisture	13,04	8,54
Volatiles	56,25	73,21
Fixed carbon	26,23	16,77
Ash	4,43	1,48
Ultimate analysis (dry basis) (wt%)		
Carbon	51,46	47,06
Hydrogen	5,46	6,82
Nitrogen	1,25	0,82
Sulfur	0,09	0,11
Ash	5,09	1,62
Oxygen (diff)	36,35	43,57
Ash composition (wt%)		
CaO	22,34	12,34
MgO	1,8	4,7
K_2O	25,56	41,65
Na_2O	1,74	0,5
Fe_2O_3	2,75	2,34
Al_2O_3	6,22	3,23
SiO_2	34,78	18,99
P_2O_5	1,77	8,81
SO_3	0,92	2,03

Due to is high potassium content, olive hust has a high propensity to cause bed agglomeration.

In terms of elements, the apparatus (see figure 4.12) is quite similar to the fluidized bed reactor described in the figure 4.3. The temperature and the pressure were measured respectively at five and three locations z from the distributor plate. The combustor was heated by means of ceramic mat heaters. The fluidizing gas was preheated to 500 °C. The

flue gas composition was also analysed by a paramagnetic and NDIR analyzers. Finally the acquisition of data (temperature, pressure and gas concentrations) was performed at a sampling frequency of 100 Hz.
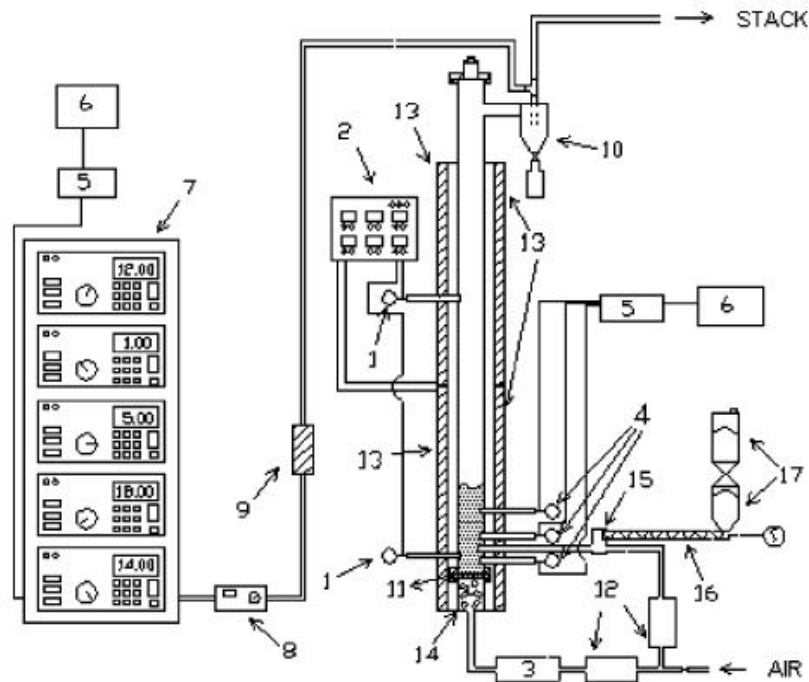
Experimental apparatus: (1) thermocouple, (2) temperature PID controller, (3) preheater, (4) thermocouple and pressure transducer, (5) acquisition data unit, (6) personal computer, (7) gas analyzers, (8) condenser, (9) filter, (10) cyclone, (11) gas distributor, (12) mass-flow controller, (13) ceramic heaters, (14) windbox, (15) fuel−air mixer, (16) screw feeder, and (17) fuel hopper.

Figure 4.12: Experimental apparatus [Scala et al., 2006]

Three temperature profiles were measured at different heights in steady-state combustion conditions (see figure 4.13) . The temperature measured at z=0,245 m is slightly lower as the other two which can be explained by the heat dispersion from the bed to colder freeboard. Till 80 minutes of experiment, the two temperatures at z=45 mm and z=145 mm are nearly the same and then they diverge (first dotted line) meaning that the combustion was concentrated in the middle section. After 174 minutes, the bed defluidized and the temperature suddenly drops for the three bed locations considered. This behaviour should be related to the decrease of heater transfer coefficients when the bed agglomeration occurs and the inhomogeneities in terms of combustion in the upper bed area.
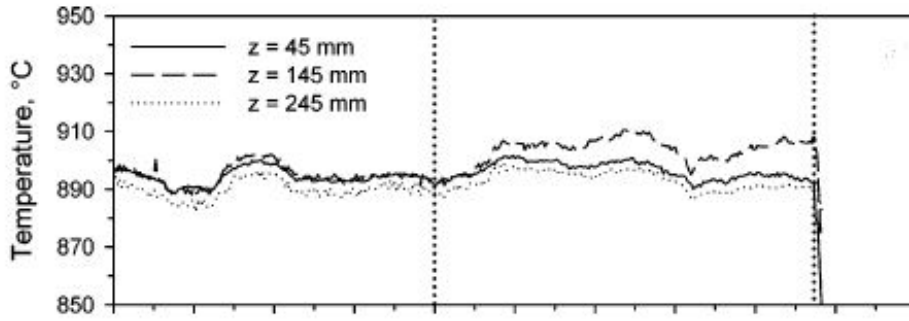
Figure 4.13: Temperature profiles at three different positions in the bed [Scala et al., 2006]

The temperature at which agglomeration happens is between 890 ℃ and 910 ℃ depending on the bed position considered. This fact supports temperature measurements in table 4.5 in terms of order of magnitude. This difference should be explained by a comparison between the olive feedstock used by [Scala et al., 2006] and the olive residue from both experiments performed (see table 4.7). Thus, the proportion of volatile is higher in the feedstock than from this thesis. We should therefore, observed a lower agglomeration temperature compared to the one from this paper which is not the case. One possibility to explain it is the difference in terms of operational conditions especially the bed temperatures which were higher in the experiments performed in this master thesis.

Table 4.7: Comparison feedstock composition with [Scala et al., 2006]

	Olive residue (from table 4.1)	exhausted husk [Scala et al., 2006]
CaO	11,86%	22,34%
MgO	6,08%	1,80%
K_2O	42,51%	25,56%
Na_2O	4,12%	1,74%
Fe_2O_3	1,19%	2,75%
Al_2O_3	2,47%	6,22%
SiO_2	12,92%	34,78%
P_2O_5	8,07%	1,77%
SO_3	5,28%	0,92%
Sum	94,50%	97,88%

During the run, pressure measurements at these three locations were also performed. After the 80 minutes, the three pressures increase due the accumulation of ash in the bed because there is no drain flow. When defluidization occurs (174 minutes), the pressures

drop suddenly because of bed channeling. Indeed, ash accumulates in the reactor and then melt, became sticky creating additional forces between bed particles which cause bed agglomeration.
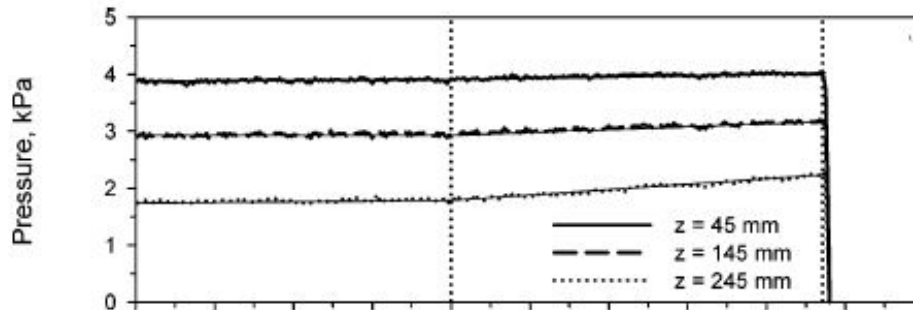
Figure 4.14: Pressures profiles at three different positions in the bed [Scala et al., 2006]

4.4 Ash melting point prediction based on ternary diagrams

The normalized element composition from the table 4.9 was reported in the different ternary diagrams (orange point) described in the chapter 3 (see figures 4.15, 4.16, 4.17, 4.18 for deformation temperature and figure 4.19 for hemispherical temperature).

The tables 4.8, 4.9 and 4.10 give the exact coordinates of the report points.

4.4.1 Ternary diagram $K_2O - CaO - SiO_2$
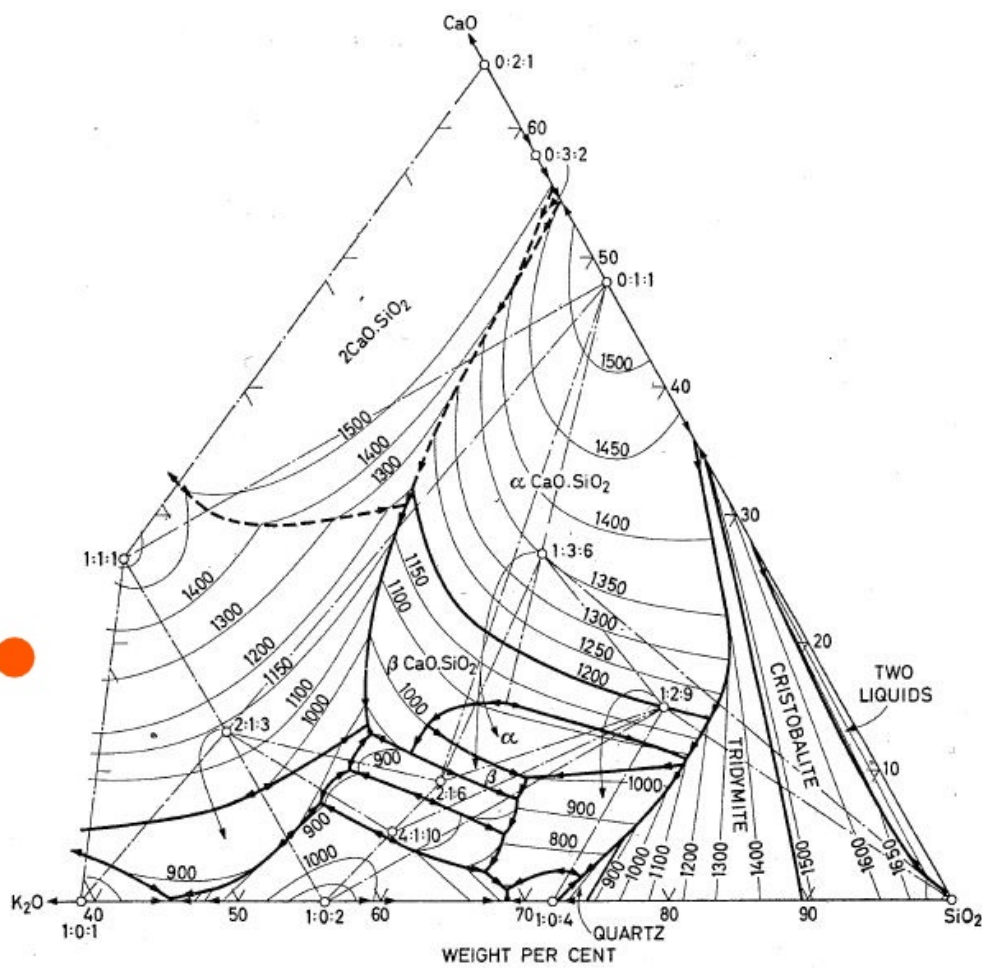
Figure 4.15: Ternary diagram $K_2O - CaO - SiO_2$ prediction [Roedder, 1959]
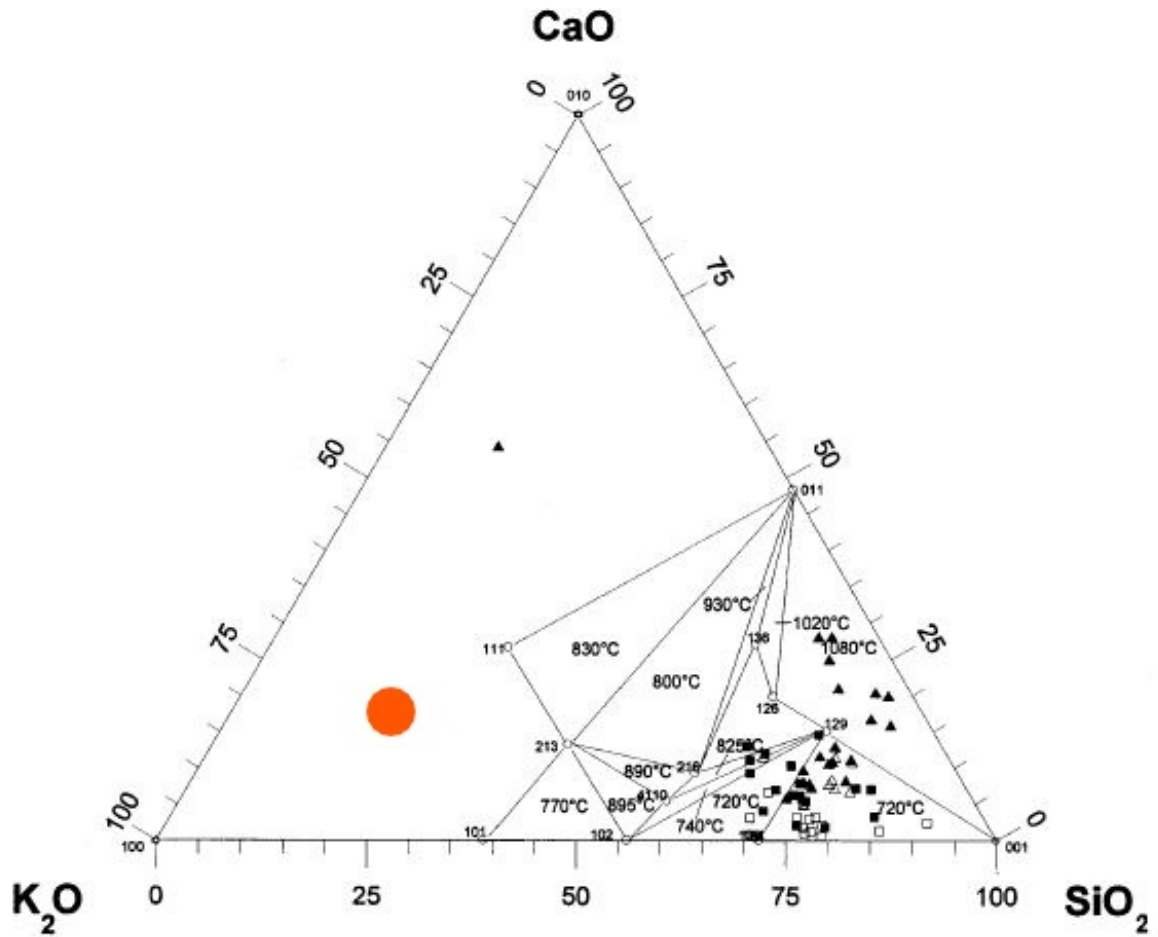
Figure 4.16: Ternary diagram $K_2O - CaO - SiO_2$ prediction [Öhman et al., 1999]

Table 4.8: Normalized compositions for $K_2O - CaO - SiO_2$ ternary diagram

Oxide	wt% from table 4.1	wt% normalized
SiO_2	12,9%	19,2%
CaO	11,9%	17,6%
K_2O	42,5%	63,2%
Sum	67,3%	100%

4.4.2 Ternary diagram $K_2O - CaO - P_2O_5$
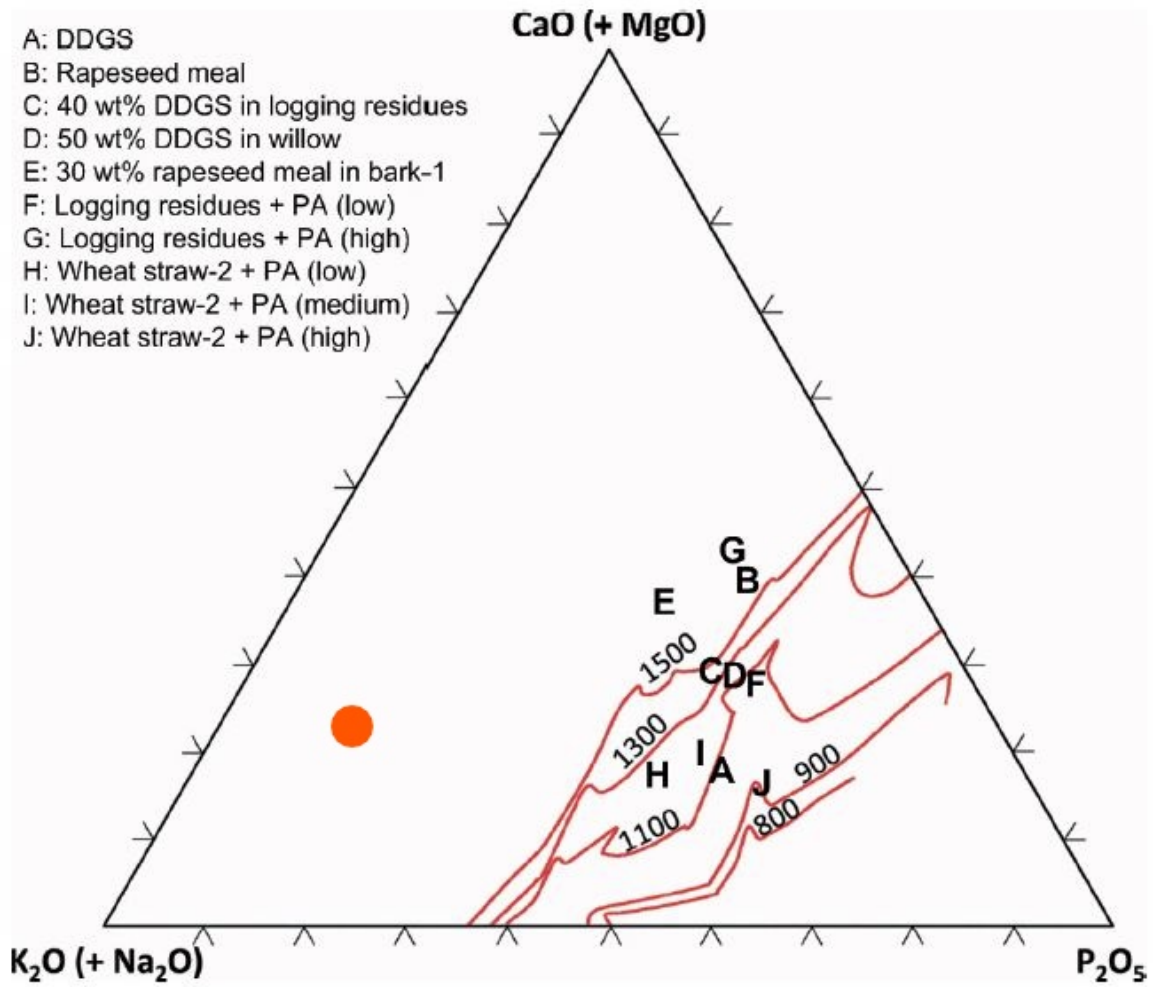
Figure 4.17: Pseudo ternary diagram $K_2O - CaO - P_2O_5$ from [Grimm, 2012] prediction

Table 4.9: Normalized compositions for $K_2O - CaO - P_2O_5$ ternary diagram

Oxide	wt% from table 4.1	wt% normalized
P_2O_5	8,1%	11,1%
$CaO(+MgO)$	18%	24,8%
$K_2O(+Na_2O)$	46,6%	64,1%
Sum	72,7%	100%

4.4.3 Pseudo-ternary diagram
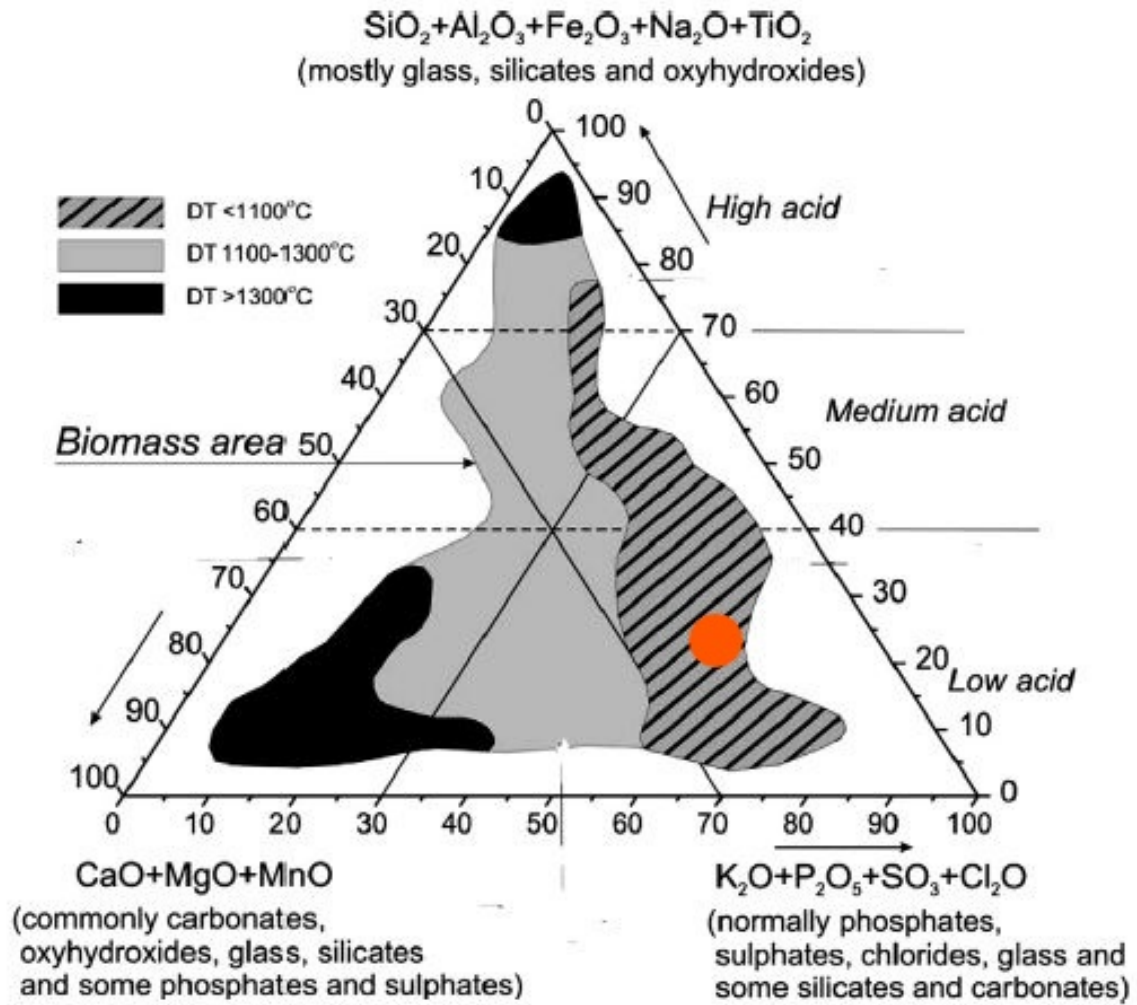
Figure 4.18: Pseudo-ternary diagram from [Vassilev et al., 2014] prediction for deformation temperature
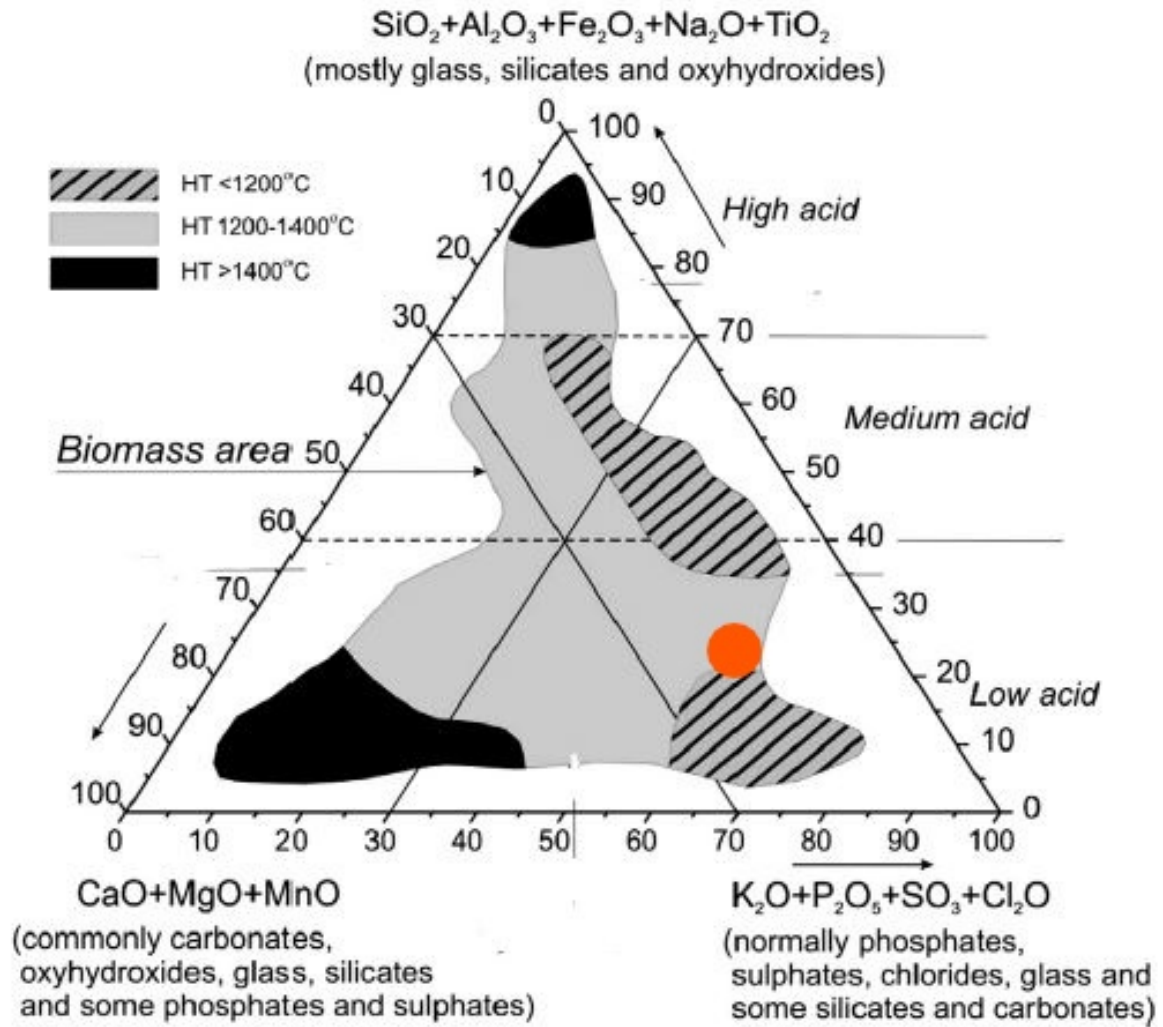
Figure 4.19: Pseudo-ternary diagram from [Vassilev et al., 2014] prediction for hemispherical temperature

Table 4.10: Normalized compositions for pseudo-ternary diagram

Oxide	wt% from table 4.1	wt% normalized
$SiO_2 + Al_2O_3 + Fe_2O_3 + Na_2O + TiO_2$	20,8%	21,2%
$CaO + MgO + MnO$	18%	18,3%
$K_2O + P_2O_5 + SO_3 + Cl_2O$	59,4%	60,5%
Sum	98,2%	100%

4.4.4 Discussion

When the number of considered components increases, the melting point predicted is decreasing because less oxides are neglected i.e. the point reported is more and more representative of the ash composition and therefore, the prediction is more accurate.

Due to the lack of available data, the melting temperature couldn't be predicted for the first three diagrams. However, we can guess that the melting point predicted is above 1000 °C which is still a big difference with experimental values from both FBC runs which are around 950 °C (see table 4.5). Pseudo-ternary diagrams predict a deformation temperature inferior to 1100 °C and hemispherical temperature between 1200 °C and 1400 °C. The weight percentage of Cl_2O needed for ternary diagram predictions has been assimilated to the weight percentage of Cl in table 4.2. As Cl proportion is quite scarce, this approximation doesn't affect much the results.

Those values predicted are in accordance with the ones determined by AFT (see figure 4.1). However, the prediction stops here. Indeed, a conclusion regarding a potential melting temperature range which would have been more useful for decision-making couldn't be reached . This underlines the need for further development.

4.5 Future considerations

The work described in this master thesis can be considered as the basis for future research projects. First of all, it would be interesting to perform the combustion of other types of biomass under the same conditons and then compare the values obtained to the ones predicted by ternary diagrams to see if they are indeed similar. Indeed, each type and sub-types of ash biomass has its own particularities due to difference of ash-forming elements content. Of course, a duplicate experiment should be the minimum to check results consistency.

Based on the previous point, it would be relevant to compared the ternary diagrams predictions to the experimental values obtained in bigger installation (scale-up) which are more representative of large scale applications.

As section 4.4.4 shows, the availability of data as well as the accuracy of the prediction is a big problem. Therefore, an emphasis has to be put on pseudo-ternary diagrams development which can address in a more accurate way slagging problems in combustion systems. Thermodynamic simulations with FactSage for example would definitely help.

Chapter 5

Conclusion

In the context of greenhouse gases reduction, biomass represents a promising alternative to fossil fuels. However, biomass has some invonvenients in combustion systems. One of those practical problems in fluidized bed reactor is bed agglomeration caused by fused ash sticking bed particles together. This phenomena is commonly called "slagging". Several solutions have been proposed to reduce the effect of slagging like additives, water leaching and co-firing.

In this master thesis, the potential of ternary diagram as prediction method for biomass slagging tendency was investigated. Ternary diagrams are generally powerful thermodynamic tools because they enable to make decision without doing any experiment. However, a preliminary literatur research showed that ternary diagrams are mostly used for classification purpose and not as an established prediction method. One of the limit of ternary diagram is first the availability of data and secondly, the prediction accuracy. Indeed, in these ternary systems the ash composition is approximated to the sum of the three main oxides. By neglecting the other components, the melting temperature predicted is generally way higher than the one measured by AFT because these components contribute to decrease the melting temperature. To circumvent that inconvenient, pseudo-ternary diagrams taking into account more elements have been developed but they are still in early ages and they need more time to gain maturity.

In the practical part, the combustion of olive pellet was performed in a lab-scale fluidized bed reactor provided by the Institute of Chemical, Environmental and Bioscience Engineering at TU Wien. The experiment was performed two times in order to check

the consistency of the results obtained. The bed agglomeration was detected at around 950 ℃ when bed temperature and pressure under the bed decrease. The pressure drop can be explained by agglomerates formation which offer a bigger counter-pressure to the air pressure. The bed temperature decreases because the combustion efficiency goes down due to agglomeration formation. The bed temperature (950 ℃) measured at the agglomeration time is between the deformation temperature (840 ℃) and the flow temperature (1400 ℃) measured by ash fusion test which is what was expected.

The next steps are to make more runs with the lab-scale fluidized bed reactor with different types of biomass and compare the results obtained with the ones predicted by ternary diagrams. The accuracy of ternary diagrams predictions should be improved by taking into account more biomass ash data and by capitalizing on simulation softwares. Therefore, the question of establishing ternary diagrams as a prediction method for biomass ash slagging propensity predictions is still opened.

Bibliography

[Arvelakis et al., 2002] S. Arvelakis, H. Gehrmann, M. Beckmann, E.G. Koukios, 2002. Effect of leaching on the ash behaviour of olive residue during fluidized bed gasification by Biomass and Bioenergy 22: 55-69.

[CEN/TS 15370-1, 2006] CEN/TS 15370-1. Solid biofuels-Method for the determination of ash melting behaviour. Part 1: Characteristic temperatures method. Österreichisches Normungsinstitut. Wien.

[Chirone at al., 2006] R. Chirone, F. Miccio, F. Scala, 2006. Mechanism and prediction of bed agglomeration during fluidized bed combustion of a biomass fuel: Effect of the reactor scale by Chemical Engineering Journal 123, 71-80.

[DIN 51730, 2007] DIN 51730. Prüfung fester Brennstoffe-Bestimmung des Asche-Schmelzverhaltens. Deutsches Insititut für Normung. Berlin.

[EU, 2001] DIRECTIVE 2001/77/EC OF THE EUROPEAN PARLIAMENT AND OF THE COUNCIL of 27 September 2001 on the promotion of electricity produced from renewable energy sources in the internal electricity market, Official Journal of the European Communities , 27.10.2001

[European Commission, 2012] Energy roadmap 2050. Luxembourg.

[Eßletzbichler, 2017] Essletzbichler, D. (2017). Auslegung, Aufbau und Inbetriebnahme einer Wirbelschichtapparatur im Labormassstab für thermische Umwandlungsprozesse von Biomasse, Technische Üniversität Wien.

[Grimm, 2012] A. Grimm. Experimental Studies of Ash Transformation Processes in Combustion of Phosphorus-Rich Biomass Fuels (2012). Lulea University of Technology, Sweden.

[Glarborg et al., 2013] Glarborg P., Jensen P.A , Dam-Johansen K., Illerup J.B., Karl-ström O., Brink A., Zevenhoven M., Huoa M., Scharler R., Brunner T., Obernberger I., Lovas T., Frandsen, F(ed) 2013, Scientific Tools for Fuel Characterization for Clean and Efficient Biomass Combustion: SciToBiCom Final Report.

[Hesse Instruments, 2016] The Heating Microscope and EMI III Software, 2016.

[Hupa et al., 2017] M.Hupa, O. Karlström, E. Vainio 2017. Biomass combustion technology development-It is all about chemical details by Proceedings of the Combustion Institute 36: 113-134.

[Jenkins et al., 1996] B.M. Jenkins, R.R. Bakker and J. B. Wei, 1996. On the properties of washed straw by Biomass and Bioenergy 10 n°4: 177-200.

[Kern et al., 2013] S.J. Kern, C. Pfeifer, H. Hofbauer. DUAL FLUIDIZED BED STEAM GASIFICATION OF COAL AND PYROLYZED COAL. Engineering Conferences International ECI Digital Archives. The 14th International Conference on Fluidization-From Fundamentals to products. 2013.

[Kohl et al., 2014] H. Kohl, H. Hofbauer, 2014. Analysenbericht über eine Brennstoff-probe. TU Wien, Prüflabor für Feuerungsanlagen am Institut für Verfahrenstechnik, Umwelttechnik und Technische Biowissenschaften.

[Lindberg et al., 2013] D. Lindberg, R. Backman, P. Chartrand, M. Hupa, 2013. Towards a comprehensive thermodynamic database for ash-forming elements in biomass and waste combustion-Current situation and future development by Fuel Processing Technology 105: 129-141.

[Nordin, 1994] A. Nordin, 1994. Chemical Elemental characteristics of biomass fuels by Biomass and Bioenergy 6 n°5: 339-347.

[Öhman et al., 1999] M. Öhman, A. Nordin, 1999. The role of Kaolin in Prevention of Bed Agglomeration during Fluidized Bed Combustion of Biomass Fuels by Energy & Fuels 14, 618-624.

[Scala et al., 2006] F. Scala, R. Chirone, 2006. Characterization and Early Detection of Bed Agglomeration during the Fluidized Bed Combustion of Olive Husk by Energy & Fuels 20, 120-132.

[Skrifvars et al., 1999] B-J Skrifvars, H.S Sorensen, L.A Hansen, F.J. Frandsen, and K D-Johansen, 1999. Characterization of Ashes and Deposits from High-Temeprature Coal-Straw Co-Firing by Energy & Fuels 13, 803-816.

[REN21, 2018] Renwables 2018 Global Status Report. Paris.

[Roedder, 1959] E. Roedder, Silicate melt systems, 1959. Physics and Chemistry of the Earth. Printed in Great Britain by Pitman Press, Bath.

[Turn et al., 1997] S. Q. Turn, C. M. Kinoshita, D. M. Ishimura, 1997. Removal of inorganic constituents of biomass feedstocks by mechanical dewatering and leaching by Biomass and Bioenergy 12 n°4: 241-252

[Van Loo & Koppejan, 2008] Van Loo S. and Koppejan J. (2008). The Handbook of Biomass Combustion and Co-firing. London 2008. Earthscan. pp 34-38, 249-267.

[Vassilev et al., 2012] S. V. Vassilev, D. Baxter, L. K. Andersen, C. G. Vassileva, T. J. Morgan 2012. An overview of the organic and inorganic phase composition of biomass by Fuel 94:1-33.

[Vassilev et al., 2014] S. V. Vassilev, D. Baxter, C. G. Vassileva, 2014. An overview of the behaviour of biomass during combustion: Part II. Ash fusion and ash formation mechanisms of biomass types by Fuel 117: 152-183.

[Wojcik et al., 2018] M. Wojcik, M. Englisch. Validation ISO/CD 21404 Solid biofuels-Determination of ash melting behavior. BEA Report 2015190, 2018

List of Figures

List of Tables